The Institute of Paper Chemistry

Appleton, Wisconsin

Doctor's Dissertation

An Autoradiographic Study of the Hemicellulose Distribution in the Walls of *Pinus resinosa* Tracheids

Erin M. Byers

January, 1989

AN AUTORADIOGRAPHIC STUDY OF THE HEMICELLULOSE DISTRIBUTION IN THE WALLS OF PINUS RESINOSA TRACHEIDS

A thesis submitted by

Erin M. Byers

B.S. 1982, State University of New York

College of Environmental Science and Forestry

M.S. 1984, Lawrence University

In partial fulfillment of the requirements
of The Institute of Paper Chemistry
for the degree of Doctor of Philosophy
from Lawrence University,
Appleton, Wisconsin

January, 1989

TABLE OF CONTENTS

ABSTRACT

The relative concentrations of lignin, cellulose, and hemicellulose vary across the wood cell wall. The relative concentration of lignin is highest in the middle lamella and primary wall while the relative concentration of cellulose and hemicellulose is highest in the secondary wall. Previous investigations of the hemicellulose distribution have relied upon fractionating the cell wall and quantitatively isolating the carbohydrates. The purpose of the present work was to visualize the distribution of hemicelluloses in their native state, directly in the cell wall.

The experimental program consisted of supplying radiolabeled hemicellulose precursors to actively growing cells within the tree. The cells metabolized the precursors and deposited them in the cell wall as radiolabeled hemicelluloses. Samples of the labeled wood were analyzed to determine the identity of the resulting labeled cell wall components. Autoradiographs were then prepared from cross sections of the labeled wood. Autoradiography is a modified photographic technique which results in the location and quantification of radioactive substances. A complex image analysis procedure was employed to determine the distribution of radiolabel across the cell wall from the autoradiographic images.

Two different hemicellulose precursors, D-(2-^{3}H)-mannose and L-(1-^{3}H)-arabinose were used. Each precursor labeled a different fraction of hemicelluloses. The D-(2-^{3}H)-mannose labeled a fraction rich in hexoses, while the L-(1-^{3}H)-arabinose labeled a fraction rich in pentoses. The distributions of radiolabel across the cell wall produced by each precursor were also significantly different.

Neither precursor produced a even distribution of radiolabel across the cell wall.

The trees which received the D-(2-^{3}H)-mannose precursor had their highest level of radiolabel in the middle of the cell wall (the S2 layer). The inner and outer cell wall layers contained much lower levels of radiolabel. Conversely, the S2 layer in the trees which received the L-(1-^{3}H)-arabinose precursor contained the lowest level of radiolabel. Higher levels of radiolabel were found in the inner and outer cell wall layers of these trees. These results indicate that the hemicelluloses are not evenly distributed across the cell wall. The hexose and pentose containing hemicelluloses are present in different proportions in each cell wall layer.

PREFACE

The thesis is divided into four main sections: Introduction, Materials and Methods, Image Analysis, and Results and Discussion. The Introduction begins with a brief description of the physical and chemical properties of the wood cell wall. This is followed by a review of published works concerning the distribution of hemicelluloses within the cell wall. The inherent strengths and weaknesses of each study are noted. Of particular interest is a discussion of the cell wall deposition of hemicelluloses in growing cells and a discussion of the effects of transitory polysaccharides. Each of these phenomena could affect the hemicellulose distributions determined by studies which have employed the analysis of developing tissues technique.

Also included in the Introduction is a statement of the thesis objectives and an outline of the experimental approach that was undertaken to achieve these objectives. The experimental approach describes the three main areas of work which were performed. Contained within this is a description of the labeled hemicellulose precursors that were chosen for this investigation and a description of autoradiography and the autoradiographic process. These descriptions provide a basis for understanding the techniques which were used in this investigation.

The Materials and Methods section is a straight forward presentation of the experimental procedures which were used. This section provides the information necessary to duplicate the procedures and includes explanations of the purposes of the experiments as they relate to the thesis objectives. The section is divided into three main areas: the preparation of labeled tracheids, the identification of the

labeled cell wall components, and autoradiography techniques.

The third section, entitled Image Analysis, begins with a theoretical discussion of the phenomena of image spread in autoradiography. The reader is provided with an understanding of how image spread occurs, how it can be measured, and how it necessitates the use of image analysis techniques for interpretation of autoradiographs. This is followed by an outline of the image analysis technique that was used in this study. Following the outline, a step by step illustration of the technique is given using data from actual autoradiographs.

The fourth section of the thesis is entitled Results and Discussion. In the first part of this section the results of the identification of the labeled cell wall components are presented. This analysis was performed to ascertain to what extent each cell wall component had been radiolabeled. These results are also interpreted in light of present knowledge of the biosynthesis of polysaccharides and lignin.

In the second part of the Results and Discussion section the results of the autoradiography analysis are presented. The distributions of radiolabel across the cell wall as determined for each set of trees by the the image analysis procedure are described. Some additional discussion of the final models proposed in the image analysis is included to clarify the results. These radiolabel distributions are then interpreted with respect to the results of the previous hemicellulose distribution studies that were presented in the literature review.

In addition to the four main sections described above are three smaller sections. These include the Conclusion, Recommendations, and Appendices. The

Conclusion presents the results of this work in a concise form. The Recommendations contains suggestions for anyone wishing to pursue future work in this area. The first three appendices contain information describing, in greater detail, some of the experimental and analytical techniques. This information, although important, was too detailed and specific to be included in the main body of the thesis. The fourth appendix contains the raw data which was collected from the photomicrographs of the autoradiographs. This data may be useful to someone who desires a more thorough understanding of the image analysis technique that was used in this investigation. It may also be of some value in the future as new and more sophisticated image analysis techniques are developed.

INTRODUCTION

THE WOOD CELL WALL

A wood cell is formed when a cambial cell divides in the tangential direction producing a xylem mother cell The tangential division of the xylem mother cell produces two xylem daughter cells each of which divide once producing a total of four cells. These ultimately develop into mature xylem cells. Xylem daughter cells are encased in primary cell walls and separated from each other by a middle lamella consisting mainly of pectin. During the first stage of their development the xylem daughter cells expand greatly in volume, and the surface area of the primary cell wall increases accordingly. Upon completion of this expansion phase the dimensions of the primary cell wall are set and the deposition of the secondary cell wall begins. The secondary wall consists of three layers: the S1 which is deposited on the inner surface of the primary wall, S2 which is the central layer, and S3 which is the inner most cell wall layer.[1]

On a structural level the wall of a fully developed lignified cell is composed of cellulose microfibrils embedded in a matrix of hemicelluloses and lignin. Lignin is a highly branched aromatic polymer made up of phenylpropane units. Cellulose is a linear polymer of D-glucose units linked β1,4. The hemicelluloses consist of a variety of polysaccharides both linear and branched. In gymnosperms the major hemicellulose is galactoglucomannan. It has a main chain of D-mannose and D-glucose units and side chains of D-galactose units and O-acetyl groups (Figure 1). 4-O-methylglucuronoarabinoxylan, the next most frequent hemicellulose in gymnosperms, consists of a main chain of D-xylose units and branches of

4-O-methyl-D-glucuronic acid and L-arabinofuranose units (Figure 1). In addition to these main hemicelluloses a number of less abundant polysaccharides exist. The structures of some are described in Table I. Theories abound as to how the hemicelluloses may be linked to both cellulose and lignin producing elaborate three dimensional networks that provide cohesiveness to the cell wall structure.[2]

Galactoglucomannan

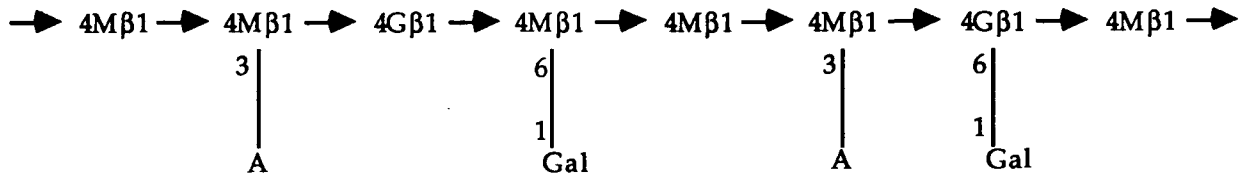

Mβ = β-D-mannopyranosyl
Gβ = β- D-glucopyranosyl

Gal = α-D-galactopyranosyl
A = O-acetyl group

Glucuronoarabinoxylan

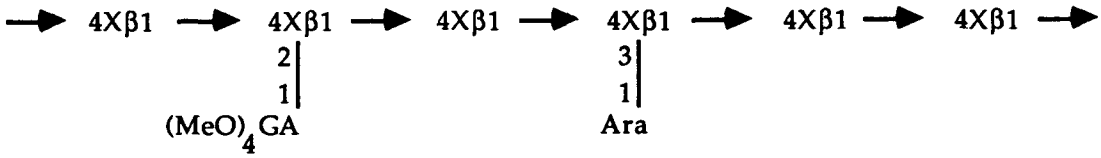

Xβ = β-D-xylopyranosyl

$(MeO)_4$ GA = 4-O-methyl-D-glucuronic acid
Ara = α-L-arabinofuranosyl

Figure 1. Structures of mannan and xylan found in gymnosperms.

Studies have shown that the relative concentrations of lignin, cellulose, and hemicellulose are not constant across the cell wall. Lignin, which can be visualized directly under ultraviolet light, has been found it to be more highly concentrated in

Table 1. Other noncellulosic polysaccharides.

NAME	MAIN CHAIN	SIDE CHAINS
XYLOGLUCAN	(β1-4)D-glucopyranose	[D-xyl$_p$] [L-ara$_p$] [L-fuc$_p$--D-galp--D-xylp]
ARABINOGALACTAN	(β1-3)D-galactopyranose	[D-galp-D-galp] [L-araf-L-araf] [D-gal$_p$] [L-araf]
PECTINS		
Galacturonic acid	(α1-4)D-galacturonic acid	
Rhamnogalacturonan	(α1-4)D-galacturonic acid, (α1-2)L-rhamnopyranose	
Arabinan	(α1-5)L-arabinofuranose	[L-araf]
Galactan	(β1-4)D-galactopyranose	

the middle lamella and primary wall than in the secondary layers.[3] The cellulose and hemicellulose conversely are more highly concentrated in the secondary layers. Unfortunately there are no direct methods for visualizing the hemicelluloses in the cell wall, as stains which react with hemicellulose also react with cellulose. Attempts to discern the concentration of hemicellulose within individual cell wall layers have therefore depended on quantitative isolation techniques. The purpose of the present work was to examine the hemicellulose distribution directly in the cell wall by first radiolabeling the hemicelluloses and then using autoradiography to detect the radiolabel distribution.

LITERATURE SURVEY

Overview

Numerous studies have been undertaken to discern the distribution of hemicelluloses across wood cell and pulp fiber walls. This survey will focus only on those which have been performed on gymnosperms. The chemical differences between angiosperm and gymnosperm cells make direct comparisons between these two divisions difficult.[4] The survey will also be limited to studies which have been performed on wood, not on pulp fibers. Chemical pulping removes much of the hemicellulose from the cell wall, and the distribution of the remaining hemicellulose within the wall may vary greatly between pulping processes.[5] Since this study is concerned with the distribution of hemicelluloses in their native state, the results of studies performed on pulped fibers have little relevance.

One of the earliest indications that the hemicellulose content may vary across the cell wall was published in 1936. In this study[6] a small fraction of pure middle lamella tissue was isolated from cross sections of Douglas fir (*Pseudotsuga menziesii*). The pentosan content of this fraction was determined to be 14% while the pentosan content of the whole wood was found to be only 5%. Later, in 1957 a technique was developed by Sultze[7] for isolating and analyzing distinct fractions of developing xylem cells from aspen wood (*Populus tremuloides*). Using this technique the hemicellulose content of individual cell wall layers was deduced from the differences seen in the monosaccharide contents of less developed cells versus more developed cells. Publication of this technique generated considerable interest in studying the hemicellulose cell wall distribution. The technique was subsequently adapted by researchers studying softwoods. The results of their work are described below.

Analysis of Developing Tissues

Meier and Wilkie[8] and Meier[9] have used Sultze's technique to study the hemicellulose cell wall distribution of pine (*Pinus silvestris* L.) and of spruce (*Picea abies* (L.) Karst.) Four fractions were isolated from each tree. Each fraction consisted of tracheids containing only certain cell wall layers: fraction 1 (M+P), fraction 2 (M+P+S1), fraction 3 (M+P+S1+part of the S2), fraction 4 (M+P+S1+S2+S3). The fractions were examined microscopically under polarized light. In this way cells which did not belong to a certain fraction could be identified and sorted out using a micromanipulator. Each fraction was subjected to a two stage sulfuric acid hydrolysis. The monosaccharides were separated by paper chromatography and quantified spectrophotometrically. The monosaccharide content of each fraction is shown in Table 2.

Table 2. Results of the analysis of developing tissue studies by Meier. Relative per cent of the monosaccharides for each fraction

Tree	Sugar	M+P	M+P+S1	M+P+S1+S2	M+P+S1+S2+S3
Spruce	Gal	17.0	9.5	3.2	1.9
	Glu	36.6	59.5	67.2	69.6
	Man	6.4	13.8	17.3	18.2
	Ara	31.7	6.3	3.8	2.0
	Xyl	8.3	10.9	8.5	8.3
Pine	Gal	20.5	8.1	3.1	3.2
	Glu	38.0	63.4	71.5	64.5
	Man	6.1	12.5	17.7	20.1
	Ara	30.8	6.9	2.0	3.2
	Xyl	4.6	9.1	5.7	9.0

The results of this study were interpreted based on the premise that any change in the concentration of a sugar from one fraction to the next higher

developed fraction was due entirely to the presence of the new cell wall layer. As an example consider the galactose content of the spruce wood. Fraction 1 contains 17% galactose (on a total monosaccharide basis) and fraction 2 contains 9.5% galactose. This was interpreted as signifying that the galactose content of the S1 layer is much lower than the galactose content of the M+P layers. Note that the comparisons are not entirely straight forward because the percentages have not been adjusted to account for the higher concentration of polysaccharides in the secondary wall relative to the compound middle lamella.

Based on this method of interpretation, the results in Table 2 show that the galactose and arabinose concentrations are highest in the M+P layers and are much lower in the secondary wall layers. The mannose content increases dramatically from the M+P layers to the S1 layer. It then continues to increase through the S2 and S3 layers but at a lower rate. The xylose content increases from the M+P layers to the S1 and then decreases from the S1 to the S2. In the spruce it remains at this decreased level in the S3 but in the pine it increases again from the S2 to the S3.

The authors also attempted to convert the monosaccharide data into the polysaccharides from which they derived. The conversion calculations were based on the reported hemicellulose structures of the time and as such are in error. The glucomannan structure used contained no galactose and many of the lesser hemicelluloses such as xyloglucan were completely unknown at the time. The authors also used the relative areas of the cell wall layers, determined microscopically, to calculate the compositions of the individual cell wall layers. The density variations between cell wall layers were not accounted for. For these reasons it is felt that the simplest form in which they presented their results (Table 2) is the most useful.

Côté *et al.*[10] also used the analysis of developing tissues technique in a study of normal and compression wood tracheids of balsam fir (*Abies balsamea* (L.) Mill.). They did not attempt to identify the S3 layer in the cell fractions. Instead they delineated fractions based on a division of the S2 layer into inner and outer halves. The results of the analysis of normal tracheids is shown in Table 3.

Table 3. Results of the analysis of developing tissue studies by Côté *et al.* Relative per cent of the monosaccharides for each fraction

Tree	Sugar	M+P	M+P+S1	M+P+S1+ S2 outer half	M+P+S1+ S2 total	Mature Wood
Fir	Gal	18.2	17.3	20.8	11.3	3.4
	Glu	43.8	57.9	55.4	61.4	66.7
	Man	5.2	14.5	15.8	18.0	20.5
	Ara	22.5	4.1	2.2	2.4	2.9
	Xyl	10.3	6.2	5.8	6.9	6.5

The relative concentrations of glucose, mannose, arabinose, and xylose within the different fractions of cells follow the same trends as were seen in the previous studies. The galactose concentrations however are quite different. In this study the galactose stays at a relatively high concentration throughout all the fractions. In the previous studies the galactose concentration was much lower in fractions which included the secondary wall. Côté *et al.* identified this difference in their results but could not explain it. They stated that the galactose trends seen by Meier were probably more reliable.

Effect of Transitory Polysaccharides

It is important to note that the interpretation of results from the analysis of developing tissues is dependent upon the assumption that once a cell wall layer is

deposited its composition does not change. Any differences seen in the next fraction are considered to be due to the presence of the new cell wall layer alone. As pointed out by Thompson *et al.*[11] this assumption may not be valid. Some hemicelluloses which are present while the cell wall is growing may not be present in the final mature tissue.

As part of a study on jack pine (*Pinus banksiana*), the polysaccharide components of holocelluloses made from mature and immature cells were investigated.[11] Three polysaccharides were isolated from the immature tissue holocellulose that were not found in the mature tissue holocellulose. The first polysaccharide was found to be similar in composition and characteristics to an "amyloid" (now know as xyloglucan) from tamarind seed. The other two polysaccharides were described as being arabinose-rich and galactose-rich respectively. Their exact structures were never determined.

Although this investigation was of a qualitative not quantitative nature the total concentration of the three polysaccharides was estimated to be at least 3.5% by weight of the immature tissue. This represents a significant concentration when coupled with the likelihood that each of these polysaccharides may be located exclusively in the primary cell wall. Why these three polysaccharides were not present in the mature tissue is not known. They may have been altered by enzymes into other polysaccharides, removed from the cell wall altogether, or have suffered some other fate. In any case, their absence in the mature tissue points out the dangers of using the hemicellulose compositions of cell wall layers in developing tissues as a measure of the compositions in the corresponding layers of mature tissues.

Effect of Hemicellulose Deposition

There are two theories concerning hemicellulose deposition. They are known as apposition and intussusception. Apposition means that the hemicelluloses are deposited on the innermost surface of the developing cell wall. Intussusception means that the hemicelluloses are deposited within a preexisting wall structure some distance from the innermost wall surface. The analysis of developing tissues technique can be valid only if the hemicelluloses are deposited exclusively by apposition. Any hemicelluloses deposited by intussusception into outer cell wall layers would be misinterpreted as belonging to the newest innermost cell wall layer. Intussusception would make the interpretation of differences between cell fractions impossible.

The evidence supporting appositional deposition of hemicelluloses is not clear. A series of pulse feeding autoradiography studies have determined the cell wall locations where tagged hemicelluloses are deposited. A study of the epidermal cells of pea stems (*Pisum sativum*) and oat coleoptiles (*Avena sativa*) by Ray [12] determined that the hemicelluloses were deposited by intussusception while the cellulose was deposited by apposition. Mullis *et al.*[13] in a study of the wood cells of aspen (*Populus tremuloides*) determined that the pentosans and cellulose were deposited by apposition. Takabe *et al.*[14] in a study of the wood cells of Japanese cedar (*Cryptomeria japonica*) determined that the hemicelluloses were deposited both by apposition and intussusception while the cellulose was deposited by apposition alone.

In light of these studies the possibility that a significant fraction of the hemicelluloses are deposited by intussusception must be considered. Consequently, the results of the analysis of developing tissues studies may not be a measure of the

hemicellulose content of individual cell wall layers. Instead they may simply represent the stages of development during which certain hemicelluloses are deposited into a preexisting wall structure. This, plus the aforementioned effects of transitory polysaccharides, requires that the results of the analysis of developing tissues studies be approached with caution.

Single Fiber Dissection

A different method has been used by Hardell and Westermark[15] to study the hemicellulose cell wall distribution. They developed a technique for dissecting single fibers into different cell wall layers. The technique starts with whole wood. The wood is chlorite delignified to approximately 97% yield. This mild delignification makes it possible to separate single fibers from the wood chips. Fibers are then dissected under a stereo microscope using specially formed tweezers. Three distinct fractions of tissue are obtained from the fibers. Fraction 1 consists of M+P layers. Fraction 2 consists of M+P+S1 layers, and fraction 3 consists of S2+S3 layers. A special procedure was developed to allow for the hydrolysis, trifluoracetate derivatization, and gas chromatography analysis of 20 nanogram quantities of these fractions. The results of a single fiber dissection analysis performed on Norway spruce (*Picea abies*) are shown in Table 4.[16]

The distribution of galactose and arabinose discerned in this study is consistent with that seen in the previous studies. Each of these sugars has its highest relative concentration in the M+P layers and lower concentrations in the secondary layers. The mannose and xylose distributions discerned by this study are markedly different than those seen in the previous studies. In this study the concentration of mannose and xylose did not change, within experimental error,

Table 4. Results of the single fiber dissection study by Hardell and Westermark. Relative per cent of the monosaccharides for each fraction.

Tree	Sugar	M+P	M+P+S1	S2+S3
Spruce	Gal	7.6±2.3	2.9±1.3	4.8±1.6
	Glu	57.4±4.3	65.9±4.1	65.0±5.2
	Man	17.6±4.0	15.5±3.6	16.2±2.5
	Ara	7.3±2.6	2.2±0.4	3.2±1.3
	Xyl	10.1±3.6	11.6±1.9	10.8±2.4

across the cell wall. This suggest that these two sugars are much more evenly distributed than the previous studies had determined.

A possible explanation for the differences seen between this study and the analysis of developing tissues studies is that this analysis was performed on fully developed mature fibers. It is therefore free of the potential pitfalls of intussusceptional hemicellulose deposition and the effects of transitory polysaccharides. This would make the results of this study seem more reliable than the others. However, the dissection of single fibers study does contain its own weakness in that a delignification step is necessary for single fiber isolation. Although this is a mild delignification and the reported yield is quite high, it still sufficiently alters the middle lamella to allow for the separation of whole intact fibers. The possibility that this delignification also alters the native hemicellulose distribution can not be ruled out.

Grinding and Density Fractionation

One other method has been used to study of the hemicellulose distribution in the cell wall. This method, developed by Whiting *et al.*[17] consists of grinding

whole wood to a fine powder and fractionating the powder according to density through a series of centrifugations. Wood chips are ground to a fine powder in a Bauer No.730 Hurricane Pulverizer. The flour is then sieved through a 500-mesh screen and the fraction that passes the screen is used for the analysis. A sample of this 500-mesh powder is dispersed in a solution of carbon tetrachloride and 1,4-dioxane in a centrifuge tube. After centrifugation, the material which remains floating is isolated. The sediment is collected and redispersed in a solution of higher density. The process is then repeated. The density of the centrifuging solution is controlled by adjusting the ratio of the two liquids.

This separation procedure was carried out on black spruce (*Picea mariana*).[18] Four distinct fractions of tissue were obtained. Three fractions consisted of tissue which remained floating after centrifugation. One fraction consisted of the final sediment after the centrifugation series was complete. According to the authors the floating fractions consisted mainly of compound middle lamella fragments. These fragments are rich in lignin and therefore less dense than fragments from the secondary wall. The fraction made up of the final sediment was thought to consist mainly of secondary wall fragments. It was denser and had a lower lignin content than the first three fractions. Each of the four fractions plus a sample of the whole wood flour were hydrolyzed with trifluoroacetic acid. Trimethylsilyl esters of the monosaccharides were prepared for quantitative gas chromatography analysis. Lignin contents of the four fractions and the whole wood flour were determined by the acetyl bromide method of Johnson *et al.*.[19]

The results of this study are difficult to interpret. Each of the analyzed fractions contains a mixture of cell wall fragments. No fraction represents a specific cell wall layer. The monosaccharide compositions of the fractions, when related to

the amount of middle lamella fragments they contain, reveal a crude hemicellulose cell wall distribution. The less dense fractions contain higher amounts of middle lamella fragments and therefore reflect the monosaccharide composition of the outer portion of the cell wall. The denser fractions are poorer in middle lamella fragments and therefore reflect the monosaccharide composition of the inner portion of the cell wall.

The results of this study are shown graphically in Figure 2. The monosaccharide composition of each fraction is plotted against its lignin content. The three fractions which remained floating after centrifuging had lignin contents of 0.60, 0.50, and 0.39 grams of lignin per gram of tissue respectively. The whole wood flour had a lignin content of 0.27 g lignin /g tissue. The fraction collected from the final sediment had a lignin content of 0.22 g lignin/g tissue. The relative concentrations of glucose and mannose decrease with increasing middle lamella content, while the relative concentrations of galactose, xylose, and arabinose increase with increasing middle lamella content.

The galactose and arabinose cell wall distributions discerned in this study are consistent with those seen in each of the previous studies. The xylose distribution discerned in this study does not correlate well with any of the previous studies. The mannose distribution follows a trend similar to that seen by Meier and Côté. The mannose concentration is lowest in the outside of the cell wall and highest in the inside. The magnitude of this gradient is not nearly as great in this study as it was in the others. The mannose content of the middle lamella is at least twice as high in this study as it was in the previous two. Note also that the distributions of mannose and xylose are not flat as predicted by Hardell and Westermark's single

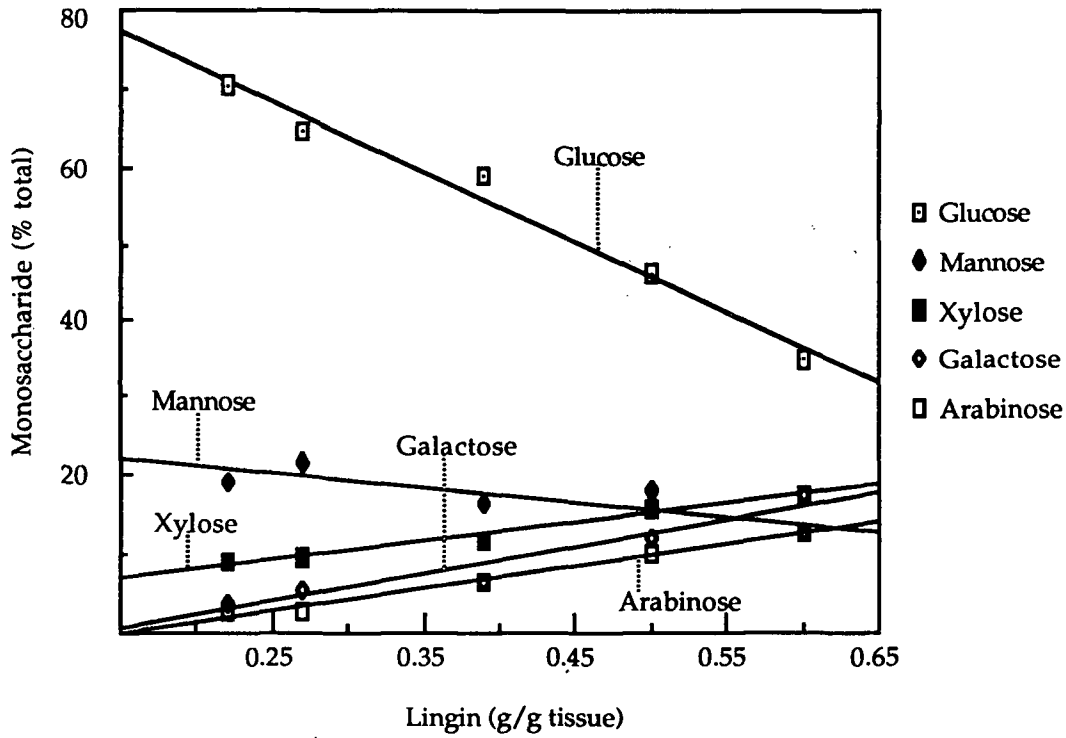

Figure 2. Results of the density fractionation study of Whiting *et al.* Monosaccharide expressed as percent of total monosaccharide vs. the lignin content of the various tissue fractions studied.

fiber dissection study.

Whiting *et al.* made an interesting comparison of their results with those of Hardell and Westermark. Based on the 57.4% glucose content of the M+P layers determined by Hardell and Westermark (Table 4), they determined the monosaccharide composition of a pseudo M+P layer in their study. The percentages of mannose, xylose, galactose, and arabinose which correspond to a 57.4% glucose content were read off their graph (Figure 2). The monosaccharide composition of the pseudo M+P layers determined in this way is very close to the actual composition that was determined by Hardell and Westermark.

When Whiting *et al.* used this same technique to compare their results to other studies, namely the spruce composition of Meier (Table 2), the fir composition of Côté (Table 3), and the monosaccharide composition of the primary walls of suspension cultured Douglas fir cells determined by Burke *et al.*[20], the comparison was quite poor. There were consistent differences seen between the pseudo M+P monosaccharide compositions of Whiting *et al.* and the related compositions found in the other studies. The pseudo M+P layers consistently predicted the mannose and xylose compositions to be too high and the galactose and arabinose compositions to be too low. As pointed out by the authors the good fit obtained with Hardell and Westermark's results coupled with the consistent differences observed with the other studies lends support to the theory that the hemicellulose content of the developing tissues is significantly different from that of mature wood.

Synopsis of Literature Studies

Based on the present literature, the nature of the hemicellulose distribution across the cell wall is somewhat uncertain. There is good evidence from all of the studies that galactose and arabinose are more highly concentrated in the ML and P layers than in the secondary wall layers. A consensus is lacking however on the cell wall distributions of mannose and xylose. The analysis of developing tissues technique has provided fairly consistent results in three studies. The technique however, is weakened by its dependence on the analysis of living cells and the associated hemicellulose compositional changes that may be occurring within them. Aside from the necessary delignification step, the single fiber dissection technique of Hardell and Westermark is the most direct and therefore possibly the most reliable. It however does not differentiate between the S2 and S3 layers. In addition to this, single fiber dissection is such an arduous task that no one, including its originators,

has attempted to duplicate the results. The technique of grinding and density fractionation is limited to the determination of gross trends. All of the fractions analyzed are necessarily mixtures of fragments from across the cell wall. The hemicellulose content of individual cell wall layers can not be determined.

THESIS OBJECTIVE

The objective of this investigation was to examine directly the distribution of hemicelluloses within the tracheid cell wall. The experimental approach consisted of supplying radioactive hemicellulose precursors to living tracheids. The cells metabolized the precursors and incorporated them into the cell wall as radioactive hemicelluloses. Electron microscope autoradiography was then used to determine the level of radioactivity in the individual cell wall layers.

EXPERIMENTAL PROGRAM

The experimental program can be divided into three main steps. Step one was to supply radioactive hemicellulose precursors to actively growing cells for an extended period of time. The duration of the feeding period had to be long enough to allow some tracheids to develop entirely, from cell division to death, in the presence of the precursor. Step two consisted of identifying the resulting labeled cell wall components to confirm that the hemicelluloses had been selectively labeled. Step three was the production and analysis of electron microscope autoradiographs from cross sections of the labeled xylem tissue.

This study differs significantly from previous autoradiography studies performed on wood in that the labeled precursors were supplied to the developing

cambium for an extended period of time. In previous studies the labeled precursor was supplied to the cambial zone in a short pulse that lasted from a few minutes to two hours. In this way, the previous studies could locate the site within the cell wall where the the label was being incorporated at that moment, and from this determine if the hemicelluloses were deposited by apposition or intussusception.

In this study it was desired to create some tracheids which had developed entirely in the presence of the precursor so that the distribution of hemicellulose across the cell wall could be discerned. The feeding period therefore had to last at least as long as the lifetime of a tracheid cell. According to Whitmore and Zahner[21] this is about four or five weeks. The feeding technique that was used to accomplish this is known as split stem feeding. It is described in detail in the Materials and Methods section.

Two hemicellulose precursors, D-(2-^{3}H)-mannose and L-(1-^{3}H)-arabinose, were selected based on a review of the literature. D-mannose has been found to be a selective precursor for D-mannosyl, L-galactosyl, and L-fucosyl units in corn (*Zea mays*)[22] and in aspen (*Populus tremuloides*)[23]. L-arabinose has been found to be a selective precursor for D-xylosyl and L-arabinosyl units in aspen (*Populus tremuloides*)[13], corn (*Zea mays*)[24], duckweed (*Lemna gibba*)[25], and strawberries (*Fragaria* Sp.)[26]. Each of the precursors were administered to separate trees in hopes of labeling two different fractions of hemicellulose. One set of trees was fed D-(2-^{3}H)-mannose in an attempt to produce tracheids containing labeled galactoglucomannan. Another set of trees was fed L-(1-^{3}H)-arabinose in an attempt to produce tracheids containing labeled 4-O-methylglucuronoarabinoxylan.

Neither of the two precursors had been tested in red pine (*Pinus resinosa*) before. It was therefore necessary to identify the resulting labeled products in this study. This was accomplished by determining the level of radioactivity in both the lignin and the individual monosaccharides of wood from trees which had received the D-(2-^{3}H)-mannose precursor and trees which received the L-(1-^{3}H)-arabinose precursor.

The final step of this thesis consisted of producing and analyzing electron microscope autoradiographs from cross sections of the labeled xylem tissue. Autoradiography is a modified photographic technique which results in the location and quantification of radioactive substances. It was invented during the first decade of this century shortly after the discovery of radioactivity.[27] During the past eighty years both the technique of producing autoradiographs and the methods of image analysis to interpret them have undergone continuous refinement. A brief discussion of the autoradiographic process is given below.

Autoradiographic Process

An autoradiograph is produced by applying photographic emulsion, that is, silver halide crystals suspended in gelatin, directly to the surface of a thin section of radiolabeled tissue. Radioactive decay particles emitted from the tissue can strike the silver halide crystals causing latent images to form in them. Upon development, any crystal containing a latent image will undergo a reduction reaction in which the silver ions in the crystal are reduced to silver metal. The silver plates out into a filamentous grain. Any crystals which have not been struck, and therefore contain no latent image, are dissolved away during the fixing procedure.

During development of an "exposed" crystal the silver grain grows in a random fashion producing a complicated shape. Note however, that the shape of the grain is unrelated to the location of the original radioactive decay event. Only the position of the grain is related to the location of the isotope. Upon viewing a developed autoradiograph in a light or electron microscope, one can see both the tissue section and the resulting silver grains on top of it. Figure 3 shows the three stages of the autoradiographic process. Figure 4 is a photomicrograph of an actual electron microscope autoradiograph produced as part of this thesis.

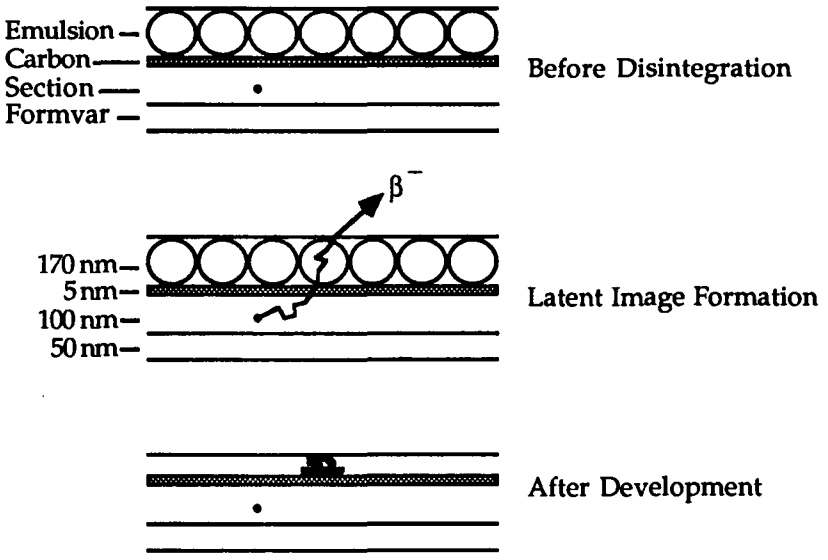

Figure 3. The three stages of the autoradiographic process.

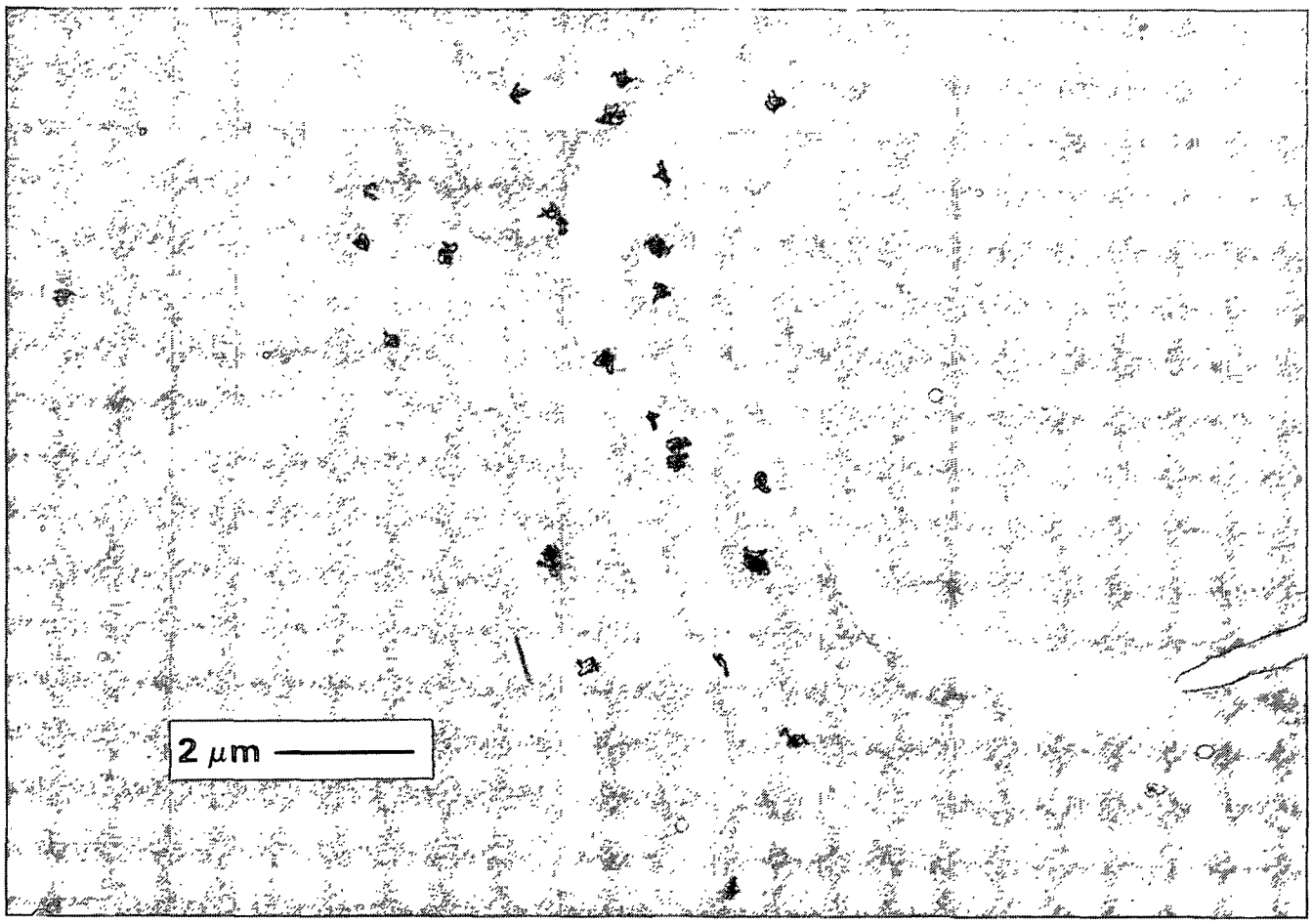

Figure 4. EM autoradiograph of Red Pine tracheids fed L-(1-^{3}H)-arabinose.

MATERIALS AND METHODS

PREPARATION OF LABELED TRACHEIDS

Plant Material

Red pine (*Pinus resinosa*) seedlings, grown from a Wisconsin seed source, were obtained from the Nekoosa Papers Inc. Nepco Nursery, Port Edwards, WI. The trees were 35 to 50 cm tall and 0.5 to 1.0 cm in diameter. They had been in seed beds for three years when they were received in the spring of 1985.

Split Stem Feeding

A split stem feeding technique was employed to supply solutions of labeled hemicellulose precursors to the cambial zone for an extended period of time. This technique had been used by other researchers to feed tomato flowers[28], pine cones and wild carrot flowers.[29] The technique is illustrated in Figure 5, and described below.

First, the needles in an area of the stem above the first whorl of branches were cut off. Then a flap approximately 1.5 inches long was cut up into the stem with a razor blade. The thickness of the flap was less than half the total thickness of the stem. A plastic culture tube approximately 0.5 inches in diameter and 1.5 inches long was inserted around the flap. The wall of the tube that fit between the flap and the main stem had been sanded smooth so that it would fit more easily and tightly into the crack. Next, a grafting rubber was tied around the tube and stem to secure the tube. A cork was inserted into the top of the tube. A notch had been cut into the cork to allow room for the flap to extend out of the tube. The wound area along the

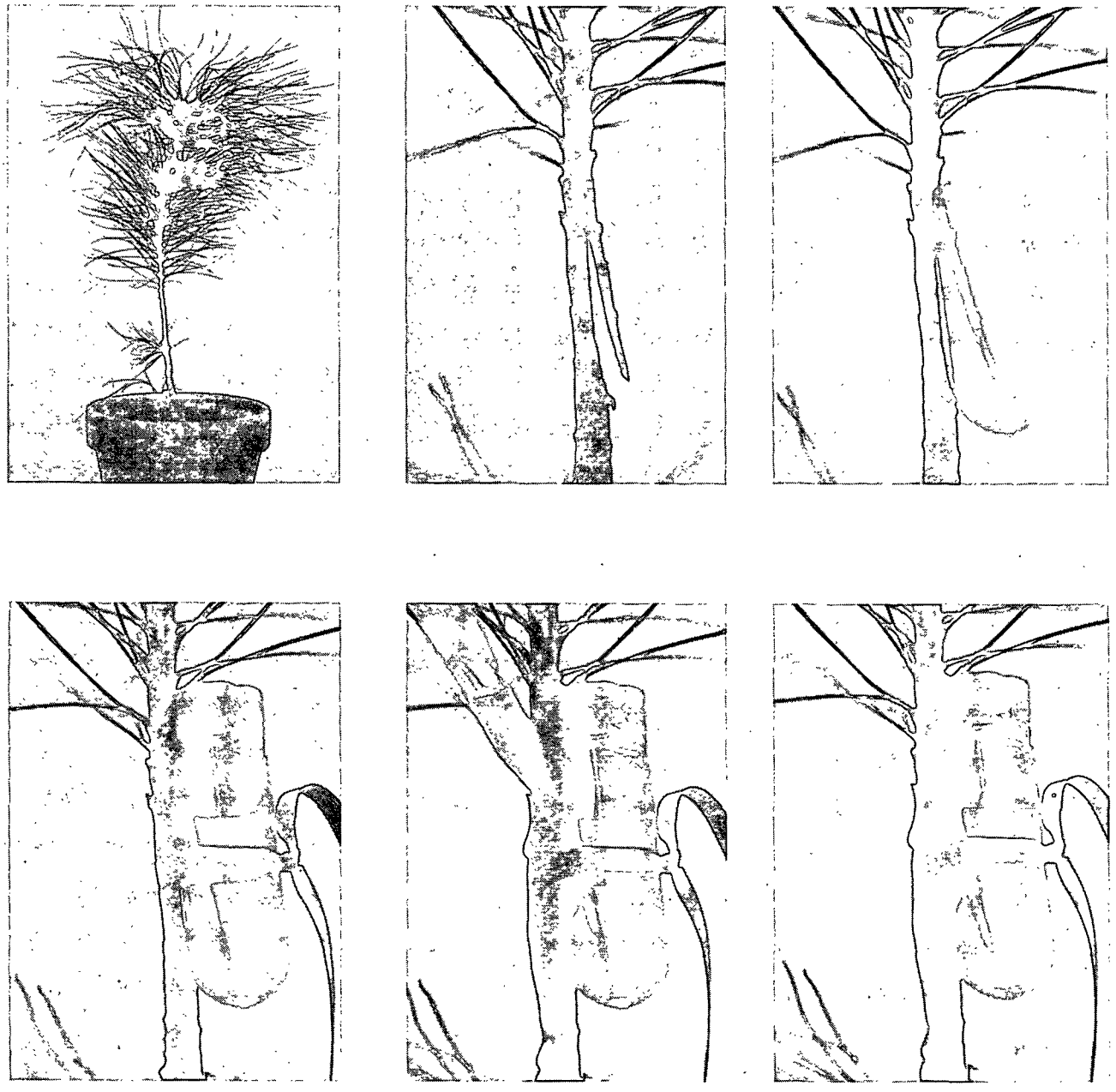

Figure 5. Split stem feeding technique.

stem and tube was then sealed with grafting wax. The cork tube interface was also sealed with wax. Two small holes were then punched through the wall of the tube to enable the insertion of a hypodermic needle so that the tube could be filled with solution.

Trees subjected to the split stem feeding technique were first fed sterile water. The feeding tube was kept full of sterile water for approximately one week. During this time the trees were assessed to see if they were responding well to the feeding technique. If a tree started to wilt or die, or if a problem occurred with the attachment of its feeding tube, it was abandoned. This rarely occurred. Trees which did well during the trial period were then given the labeled sugar feeding solutions.

Radiochemicals and Dosages

Solutions of the tritiated hemicellulose precursors in sterile water were obtained from outside suppliers. Three different lots of D-(2-^{3}H)-mannose, with specific activities of (14.5 Ci/millimole), (23.5 Ci/millimole), and (30 Ci/millimole) respectively, were obtained from New England Nuclear Corp. Boston, Mass. USA. A custom order of L-(1-^{3}H)-arabinose (2 Ci/millimole) was obtained from Amersham Corp. Arlington Heights, IL. USA. In the D-(2-^{3}H)-mannose the tritium atom was attached to the two position carbon. In the L-(1-^{3}H)-arabinose the tritium atom was attached to the one position carbon.

Separate feeding solutions were prepared for each tree. Since an extended feeding study of this nature had not been done previously, the concentration of radioactivity in a feeding solution which would produce a degree of labeling in the cell wall suitable for autoradiography and radioassay was unknown. A range of

solution concentrations were selected based on the following criteria: the solution uptake rate of the feeding flap of each tree, the radioactivity concentration of solutions used in previous pulse feeding studies, and the economic factor of consuming expensive radioactive chemicals.

The solutions were prepared in sterile 50 ml hypovials. Sterilized water was used for the dilutions. When starting a tree on a feeding solution, all of the test water was withdrawn from the feeding tube via a long hypodermic needle inserted through one of the two holes in the wall of the tube. The tube was then filled with the tritiated sugar feeding solution. The trees were checked at least once a day to insure that there was feeding solution in their tubes and that their feeding flaps were saturated. When necessary, additional feeding solution was added to the tubes. The feeding solutions, contained in the 50 ml hypovials, were stored in a refrigerator at 2°C when not being used. Table 5 lists the duration of the feeding period and the dosage of radioactivity received by each tree. Trees containing a prime mark in their number were fed during summer 1986. All others were fed during summer 1985.

Isolation of Tissue

Following the completion of its feeding period each tree was dissected. The base of the stem was severed just above the soil and all of the needles were removed. The stem and branches were then cut into 3 cm segments and stored in aqueous 30% methanol at 2°C in a refrigerator. Each stem and branch segment was stored in a separate vial. Each segment was catalogued so that the exact location within the tree from which it originated could be determined.

A stem segment 0.5 cm long located 0-3 cm above the feeding flap was taken

Table 5. Red pine split stem feeding data.

Tree	Precursor	Specific Activity (Ci / mM)	Solution Concentration (mCi / mL)	Volume Uptake (mL)	Total Dose (mCi)	Feeding Period (days)
2	ARA	2	0.048	23.1	1.1	60
4	ARA	2	0.017	36.1	0.6	61
5	ARA	2	0.019	38.3	0.7	62
8	ARA	2	0.122	18.9	2.3	54
1'	ARA	2	0.167	33.6	5.6	46
3	MAN	14.5	0.016	37.2	0.6	61
6	MAN	14.5	0.029	18.7	0.5	62
7	MAN	30.0	0.156	24.7	3.9	53
4'	MAN	14.5	0.060	40.4	2.4	46
5'	MAN	23.5	0.100	14.9	1.5	48

from each tree for autoradiography. These segments were quartered axially and then washed three times (for 4 hours each time) with ice cold solutions of the unlabeled precursor (1g/l) in aqueous 30% ethanol. The trees which had been fed D-(2-^{3}H)-mannose were washed with solutions of D-mannose. Those which were fed L-(1-^{3}H)-arabinose were washed with solutions of L-arabinose.

These washings were done as a precaution to remove any unmetabolized tritiated precursor that may have been present in the tissue. The procedure used was based on that of Mullis.[23] The segments were then washed with aqueous 30% ethanol, containing no sugar, overnight. Following this, the quartered segments were dehydrated by progressive solvent exchange into 100 % acetone according to the schedule in Table 6.

Table 6. Acetone dehydration of stem segments.

Acetone concentration (% in water)	Time in solution
30 %	1 hour
50 %	1 hour
70 %	1 hour
90 %	1 hour
100 %	several days

For the identification of labeled cell wall components, a stem segment approximately 3 cm long located 2-6 cm above the feeding flap was taken from each tree. The bark was removed from these segments and the outer most growth ring was cut away with a scalpel. This outer most growth ring was then subjected to the same washing and dehydration procedures as the tissue for autoradiography.

IDENTIFICATION OF THE LABELED CELL WALL COMPONENTS

Hydrolysis of Labeled Wood

This hydrolysis was performed on samples of wood from the outer most growth ring. After this wood had been washed and acetone dehydrated it was allowed to air dry. It was ground in a mini Wiley mill over a 20 mesh screen (20 bars per inch). Much of the sample remained as particles too large to pass the screen. The effectiveness of the Wiley mill is greatly reduced when very small quantities of material (10 to 30 mg) are used. As a result, some particles too large to pass a 20 mesh screen were included with those that did pass the screen in the final sample for hydrolysis.

Ten to 20 mg samples of this ground wood were subjected to a two stage hydrolysis procedure based on that of Saeman *et al.*.[30] The primary hydrolysis was carried out in a 50 ml beaker on a dry block heater at 30°C for 1 hour. 25 ml of 72 % sulfuric acid per gram of wood were used. During this stage the wood particles were mixed and firmly ground with a 5 mm diameter glass stirring rod to aid the penetration of the acid. After one hour additional water was added to dilute the acid solution to 2.5 %. The beaker was then covered with aluminum foil and placed into an autoclave at 121 °C for one hour for the secondary hydrolysis.

Following the secondary hydrolysis, the solution was filtered through a Millipore filter type HA (mean pore size of 0.45 μm) to isolate the Klason lignin. The filter paper and the lignin were washed repeatedly with water and then dried in a desiccator over phosphorus pentoxide. The filtrate, consisting of the hydrolyzate and the water that was used to wash the lignin, was neutralized with an excess of barium carbonate. The resulting barium sulfate was allowed to settle overnight. It was then removed by filtering the solution first through a freshly prepared mat of fiberized Whatman no.1 filter paper and then through a Millipore type HA filter. Dowex 50W-X8, H^+ ion exchange resin was added to the filtrate to remove any excess Ba^+ ions.

The ion exchange resin was later removed by filtering the hydrolyzate through a coarse sintered glass funnel. To prepare the hydrolyzate for chromatography, it was evaporated to dryness in a 50 ml pear bottom flask under reduced pressure on a rotary evaporator at temperatures not exceeding 40°C.

Preparative Layer Chromatography

Water was added to the dried pear bottom flask to bring the concentration of the hydrolyzate to 50 mg/ml. It was found that this concentration was the maximum that could be applied to the chromatography plates and still achieve adequate resolution of the monosaccharides. The volume of the dilution water was based on the original weight of the ground wood before hydrolysis minus the weight of its dried Klason lignin.

Based on the work of Iwakawa *et al.*[31], a chromatography system using silica gel coated plates and an irrigant of ethyl acetate - pyridine - water in the volume ratio of 8 - 2 - 1 was chosen to separate the hydrolyzate into individual monosaccharides. Preparative layer plates, 20 X 20 cm glass plates coated with 2 mm of silica gel 60 without fluorescent indicator, produced by E. Merck, Darmstadt, G.F.R., were purchased from Brinkman Instruments, Westbury, NY. Before spotting, the outer 2 - 3 mm of silica gel were scraped away from the bottom and side edges. The hydrolyzate was spotted along a horizontal line 1.5 cm from the bottom edge of the plate. A line of fifty slightly overlapping spots, 1 µl each was applied to the plate using a 10 µl syringe. On each side of this line of spots were applied two additional spots, also 1.5 cm from the bottom edge of the plate. The resolved monosaccharides from these spots were later used as markers to locate the bands of resolved monosaccharides between them. After spotting, the plate was allowed to dry for 3 to 4 hours before it was developed.

Development was carried out in a glass tank 22 X 22 X 10 cm. The tank had a ground glass lid which was sealed with vacuum grease. It was filled to a depth of 0.7 cm with the irrigant. Whatman no. 1 filter paper was used to line the inside of the

10 cm wide walls. The filter paper which extended into the irrigant helped to saturate the tank atmosphere. The tank was allowed to equilibrate for a minimum of 2 hours before a plate was placed in it. Each plate was developed three times in the same direction. Development was stopped when the solvent front had risen to the top of the plate. The plates were air dried in a flat position for 8 to 10 hours between developments. Fresh irrigant and filter paper were used for each development.

When a plate had dried after its final development, it was sprayed with a 3 % solution of p-anisidine hydrochloride in n-butanol.[32] The spots, and the area above them, that were on either side of the line of 50 spots were sprayed. The line of fifty spots and the area above it were covered by a glass plate to protect it from the spray. Immediately after spraying the plate was placed into an oven at 105 °C for 5 min. Upon heating, this reagent undergoes a color producing reaction with carbohydrates. The resolved monosaccharides were then located by viewing the plate under UV light.

Horizontal bands corresponding to the bands of resolved monosaccharides from the original 50 spot line were delineated by referring to the visible, resolved monosaccharides on either side of them. It was desired not to directly spray the resolved bands because the resulting colors would later interfere with the liquid scintillation counting of the monosaccharides.

Isolation of Monosaccharides for Liquid Scintillation Counting

Bands of silica gel containing the resolved monosaccharides (galactose, glucose, mannose, arabinose, and xylose) and the original line where the hydrolyzate had been spotted, were scrapped off the plates using a scalpel and razor

blade. The isolated silica gel bands were placed in separate 150 ml beakers with 80 ml of water and a teflon stir bar. The samples were stirred to break the large pieces of silica gel into small particles. The beakers were then covered with parafilm and placed in a refrigerator at 2°C. Twenty four hours later the samples were taken out, the settled silica gel was stirred up, and the samples were returned to the refrigerator. Twenty four hours after this the samples were filtered through Whatman 934-AH glass fiber filters supported by a coarse sintered glass funnel, to remove the silica gel.

The solutions were then transferred to 300 ml freeze dry bottles, shell frozen in a dry ice-acetone bath, and freeze dried. After drying, the contents of the freeze dry bottles, consisting of the monosaccharides plus some inorganic binder remaining from the silica gel, were transferred to Wheaton 180 liquid scintillation counting vials. The contents were transferred by repeatedly washing the bottles with water and then pipetting the water into the scintillation vials. Approximately 12 ml of water were used for each sample in this stage. The vials were frozen in a freezer and placed in a bell jar for freeze drying. After drying, 10 ml of liquid scintillation cocktail (Solvent-Free LSC medium, Isolab, Inc. Akron, OH.) were added to each vial. The vials were then counted in a Beckman LS3801 liquid scintillation counter.

Liquid Scintillation Counting

In addition to the monosaccharides, samples of Klason lignin were also counted. Samples of lignin were placed directly into scintillation vials with 10 ml of cocktail. Both the lignin and monosaccharides were counted to a predetermined 2 sigma value of 10. The 2 sigma value establishes the 95% confidence level for the

count and depends on the total number of counts recorded. Thus, a 2 sigma value of 10 means that in 95 out of 100 times a sample is counted, the counts per minute (CPM) determined will be within ± 10 % of the mean. Five out of 100 times the CPM determined will be outside that 10 %. This does not indicate instrument variability. Instead, it results from the randomness of the radioactive decay process.

The CPM determined for each sample were converted to disintegrations per minute by a predetermined quench curve. CPM is a measure of the rate of activity observed by the instrument. Disintegrations per minute (DPM) is a measure of the absolute activity taking place within the sample. CPM differs from DPM because not all emitted radioactive decay particles interact with the cocktail to produce light. Some particles may be absorbed by the solvent before they can react with a fluor molecule. This phenomenon is known as quenching. The amount of quenching occurring within a sample was automatically determined by reference to a standard of known radioactivity contained within the instrument. The quench curve, established as part of this thesis, determined the DPM of a sample from its measured CPM and its measured degree of internal quenching. The details of the construction of the quench curve are given in Appendix I.

Test for the Presence of Unmetabolized Precursor

The purpose of the autoradiography work was to determine the distribution of radioactive hemicelluloses across the cell wall. If a significant quantity of unmetabolized D-(2-^{3}H)-mannose or L-(1-^{3}H)-arabinose remained in the cell wall it would have obscured the distribution of radioactive polymer. An experiment was performed to determine if a significant amount of unmetabolized radioactive precursor remained in the xylem tissue.

The experiment consisted of reducing samples of wood from the outer most growth ring with sodium borohydride. This caused the free sugars, including the tritiated precursors and the reducing ends of polysaccharides, to be reduced to their alditol forms. Following this, the wood was subjected to the normal hydrolysis, preparative layer chromatography, and liquid scintillation counting procedures discussed before.

The preparative layer chromatography completely separated L-arabinose from L-arabitol and D-mannose from D-mannitol. The radioactivities of D-mannose and L-arabinose determined by liquid scintillation counting were therefore free from any contributions of unmetabolized D-(2-^{3}H)-mannose and L-(1-^{3}H)-arabinose. The radioactivities of D-mannose and L-arabinose from unreduced wood were then compared with those of reduced wood to determine if umetabolized tritiated precursors had contributed to their radioactivities. The details of the sodium borohydride reduction procedure and the PLC separation of alditols and aldoses are given below.

Wood from the outer most growth ring was washed, acetone dehydrated, and ground in Wiley mill according to the procedures described before. To reduce this wood it was first necessary to rehydrate it. This was accomplished by soaking the wood in water in an evacuated desiccator. A vacuum was drawn and released several times before finally being drawn down and sealed. The desiccator containing the ground wood in a beaker of water was placed in a refrigerator at 2°C for 5 days.

After this time the water was drawn off through a pipette and 25 ml of a

0.25 M sodium borohydride solution were added. The beaker was then placed inside a desiccator (not under vacuum) in a cold room at 5°C. The reduction was stopped 5 days latter by the addition of 5 ml of 3 M acetic acid. The solution effervesced indicating that some unreacted borohydride still remained. The solution was then filtered through a Millipore filter type HA. While on top of the filter, the sample was washed with 300 ml of distilled water. This borohydride reduction was adapted from a procedure that Gentile[33] used to reduce cellulose. From this point on the sample was hydrolyzed, chromatographed, and counted according to the procedures outlined before.

The preparative layer chromatography technique described earlier was tested and found to provide adequate separation of D-mannose and L-arabinose from their corresponding alditols. The experiments showed that D-mannitol resolved at the same point as D-galactose and would be included with this sugar when it was isolated from the plate. L-arabitol resolved between D-glucose and D-mannose and would be included with these sugars when they were isolated from the plate. Appendix II lists the results of thin layer chromatographic separation of the monosaccharides and their corresponding alditols.

AUTORADIOGRAPHY TECHNIQUES

Embedding and Sectioning

The acetone dehydrated quartered stem segments were embedded in Spurr's resin. Fresh resin was prepared according to the composition listed in Table 7.

Table 7. Composition of Spurr's embedding resin.

vinyl cyclohexene dioxide	10 g
DER 736 resin	6 g
nonenyl succinic anhydride	26 g
dimethylaminoethanol	0.4 g

The stem segments were removed from vials containing 100% acetone and placed in embedding capsules containing 50% acetone and 50% Spurr's resin. The segments remained in this mixture for 24 hours. This mixture was then pipetted off and replaced with 100% Spurr's resin. The capsules were stored in a desiccator under vacuum for 24 hours. After this period the 100% Spurr's resin was replaced with fresh 100% Spurr's resin. The capsules were kept under vacuum for an additional 72 hours and were then placed in an oven at 70°C for 15 hours to cure.

The embedded stem segments were sectioned on a Sorvall MT2-B ultramicrotome with a diamond knife. For light microscope autoradiography, 400 nm thick sections (corresponding to the secondary violet interference color) were taken. The sections were expanded with trichloroethylene vapor prior to

determining their thickness. They were then mounted on formvar coated glass slides. For electron microscope autoradiography, sections 100 nm thick corresponding to the primary gold interference color (measured after expansion with trichloroethylene vapor), were taken. These sections were mounted on formvar coated 200 mesh grids (200 lines/inch). Both nickel and gilded nickel grids were used.

Production of Light Microscope Autoradiographs

The sections, mounted on microscope slides, were coated with a thin layer of carbon (approximately 5 nm) in a Denton DV-502 vacuum evaporator. The layer thickness was judged by the deposition of carbon on a piece of white paper that was positioned adjacent the slides in the evaporator. The carbon evaporation was stopped immediately after the paper began to darken. The carbon layer provides a homogeneous surface on which to apply the autoradiographic emulsion. It also serves as a barrier to chemical interactions between the section and the emulsion.

The sections were then coated with a layer of Ilford L4 autoradiographic emulsion, using the method of Gould *et al.*[34]. Ilford L4 was melted in a water bath at 45°C. Fifty ml of water, containing 10 drops of glycerol, were heated in the same water bath. Five ml of melted Ilford L4 at 45°C and 20 ml of water and glycerol also at 45°C were mixed together in a 30 ml beaker. The beaker was allowed to equilibrate to the room temperature of 20°C. During this time, it was stirred slowly with a glass rod for 9 minutes. The beaker was then covered with parafilm and inverted three times. At this point the slides were dipped into the solution by hand and withdrawn at an even rate. The slides were dried in an upright position. Ilford L4 emulsion is light sensitive so all of the above procedures were performed in a dark room under Kodak 1A safe light illumination.

Blank slides which had been coated with formvar and carbon but contained no sections were coated first. After drying, these slides were then taken out of the dark room and inspected under normal light. It was desired that the slides be coated with a layer of emulsion at least 170 nm thick. This thickness corresponds with a slightly overlapping monolayer of silver halide crystals and produces a violet interference color under white light.[35] If the layers on the test slides were found to be at least 170 nm thick, then slides containing the sections were coated in the same manner. Approximately 40 slides could be coated from one 25 ml batch of emulsion dipping solution. The layer thickness was checked periodically by dipping and inspecting a blank slide after every 5 or 10 section containing slides.

After drying, the section-containing slides were placed in plastic slide boxes along with Dricap desiccating capsules (Ted Pella, Redding, CA.). The boxes were sealed with black electrical tape and completely covered with two layers of aluminum foil to make them light proof. They were then stored in a refrigerator at 2°C. After the duration of the exposure period (1 to 6 weeks), the slides were returned to the dark room and developed.

The development procedure is listed in Table 8. The times listed are for a room temperature of 20°C. The times of developing and fixing were adjusted to the actual darkroom temperature on the day of development. The times were decreased by 15 seconds for every degree above 20°C or increased by 15 seconds for every degree below 20°C.

Table 8. Development of light microscope autoradiographs.

Procedure	Solution	Time
development	Kodak D-19 (diluted 1 : 2 with water)	4 min
stop bath	1% acetic acid	10 sec
fix	Kodak Rapid Fixer	5 min
wash	distilled water	3 min
wash	distilled water	2 min
wash	distilled water	1 min

Seventy ml of each solution were contained in 150 ml beakers. The slides were developed two at a time. The light microscope autoradiographs were observed with a Zeiss Photomicroscope II using phase contrast optics. Inspection of these autoradiographs accomplished two things. First, it determined which embedded stem sections contained sufficient radioactivity for autoradiography. Second, the exposure period necessary to produce an LM autoradiograph with a sufficient number of grains was used to gauge the necessary exposure period for an EM autoradiograph made from the same block.

Production of Electron Microscope Autoradiographs

EM autoradiographs were produced using a modified version of the looping technique originally developed by Caro and Van Tubergen[36] and later refined by Williams[37]. This technique consisted of preparing a membrane of gelled autoradiographic emulsion and then applying this membrane directly to the surface of the tissue section. EM autoradiographs can not be made by applying liquid

emulsion to sections mounted on grids. Layers produced by applying liquid emulsion to grids have very uneven distributions of silver halide crystals. Large gaps between the crystals are unacceptable because much of the radioactivity of the tissue underneath these gaps would go undetected.

As a necessary first step of the looping technique, the grids containing the 100 nm thick sections were mounted on cork stoppers. A piece of doubled sided tape was applied to the narrow end of a number 2 cork. A hole, slightly smaller than a grid was punched through the tape. The grid was then stuck to the tape, with the section side exposed. Because of the hole in the tape, the grid was stuck only by its outer most edges. This was important in that later in the procedure it was necessary to remove the grid from the cork without damaging it. The corks were placed inside a Denton DV-502 vacuum evaporator and the EM sections were coated with a thin layer of carbon in the same manner as the LM sections.

After carbon coating the samples were moved to a darkroom for the application of the emulsion layer. The darkroom conditions had to be carefully maintained for the looping technique to work. The temperature was kept between 18 -20°C. The best results were obtained at 18°C. The relative humidity was kept as close to 50% as possible. Again, Kodak 1A safelight filters were used for illumination.

The autoradiographic emulsion was prepared for the looping technique in the following manner. Seven and one half grams of Ilford L4 autoradiographic emulsion were weighed into a 250 ml beaker. Fifteen ml of distilled water were added to the beaker. It was then placed in a water bath at 45°C. It was stirred lightly with a glass rod for 10 minutes to melt the emulsion. Three tenths ml of an

aqueous 2% dioctyl sodium sulphosuccinate solution (a surfactant trade named Manoxol OT/P, Polysciences Inc., Warrington, PA.) was added to the beaker.

The solution was stirred slowly in the water bath for 5 more minutes. It was then placed directly into an ice bath for 3 minutes where it was stirred continuously but slowly. After this time the beaker was placed directly on the lab bench for 20 minutes. During this time it was lightly stirred almost continuously with a glass rod.

The emulsion was now ready for looping. A 3 cm diameter loop of 20 gauge nichrome wire attached to a glass handle was submerged into the emulsion. It was withdrawn edge first. At this point the loop contained a thin film of emulsion that was not quite solid. After a few seconds, the film gelled into an elastic membrane. This membrane was now ready to be applied to a grid. A cork stopper was placed on the lab bench, grid side up. The loop was passed down over the cork. The membrane first stretched and then broke, covering the surface of the grid and the top of the cork. Figure 6 illustrates this procedure.

A batch of emulsion produced good membranes in this manner for about 40 minutes. After this time the emulsion became too stiff and the membranes became too thin. The quality of the resulting emulsion layers were monitored throughout this time. After every 5 or 10 section containing grids, one blank formvar coated grid was coated. These blank grids were then observed in the transmission electron microscope to assess the quality of the emulsion layer. An acceptable emulsion layer was one that contained a slightly overlapping monolayer of silver halide crystals.

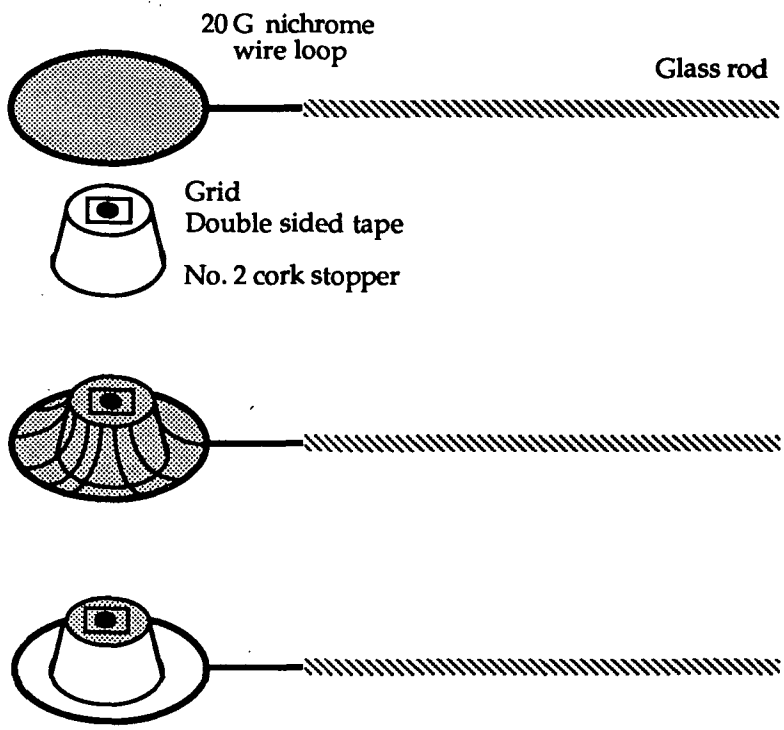

Figure 6. Application of gelled membranes of autoradiographic emulsion to electron microscope grids.

Approximately 16 sample-containing grids were coated with one batch of emulsion using this technique. After coating, the corks were inserted (grid side in) into 1 inch lengths of tygon tubing. One cork was inserted into each end of the tube. In this way, the surface of the corks containing the grids were protected from contact. The corks in tubes were then placed in plastic slide boxes along with Dricap desiccating capsules. The boxes were sealed with black electrical tape and completely covered with two layers of aluminum foil to make them light proof. They were then stored in a refrigerator at 2°C. After the duration of the exposure period (5 - 16 weeks), the grids were returned to the dark room and developed.

The development schedule is listed in Table 9. The times listed are for a

room temperature of 20°C. The times of developing and fixing were adjusted to the actual darkroom temperature on the day of development. The times were decreased by 7.5 seconds for every degree above 20°C or increased by 7.5 seconds for every degree below 20°C. Drops of each solution were placed on a piece of parafilm. The grids were carefully removed from the corks with tweezers and then floated section side down of the surface of the drops. Each grid was developed on fresh drops. The grids were dried by touching the outer edge of the grid to a piece of tissue paper. After drying, the grids were observed in a JEOL JEM-100CX II electron microscope operated in the transmission mode.

Table 9. Development of electron microscope autoradiographs.

Procedure	Solution	Time
development	Kodak D-19 (undiluted)	2 min
stop bath	1% acetic acid	30 sec
fix	25% sodium thiosulfate	3 min
wash	distilled water	2 min
wash	distilled water	2 min

Controls for Positive and Negative Chemography

Positive chemography can occur when the tissue section contains chemicals which induce latent image formation in the silver halide crystals by direct chemical action. This is a very rare phenomenon in EM autoradiography. The use of a carbon layer between the section and emulsion makes the possibility of this occurring even more unlikely. The occurrence of positive chemography can be easily detected by preparing autoradiographs of unlabeled tissue. These

autoradiographs should contain no developed silver grains. If they do, then positive chemography would be suspected. No effects of positive chemography were encountered in this work. Numerous autoradiographs were produced from stem sections which produced no developed silver grains.

Negative chemography is the removal of latent images from the silver halide crystals by chemicals contained in the tissue section. It is also rarely occurs in EM autoradiography. Controls were produced to test for the occurrence of negative chemography in this work. EM autoradiographs were produced in the normal way. They were then removed from the dark room and exposed to light in order to fog the entire emulsion layer. The autoradiographs were then returned to the darkroom, stored and eventually developed in the normal manner along with the regular autoradiographs. These control autoradiographs were then inspected in the electron microscope. If negative chemography had been occurring, areas with no silver grains or with greatly reduced silver grain densities would have been observed. No such areas were found, indicating that negative chemography was not occurring in this system.

Background Determination

The background level of an autoradiograph is the concentration of silver grains which results from sources other than the decay of radioactive atoms in the section. Possible sources of background include light contamination in the darkroom, light contamination during storage, exposure of the autoradiographs to other sources of radiation prior to development, and exposure of the autoradiographic emulsion to light prior to its use. Background silver grains can also result from the development process. All developers will cause a certain small percentage of unexposed silver halide crystals to be developed. If an autoradiograph

is left in contact with the developer for an excessive period of time, the fraction of unexposed crystals which are developed can become significant.

The level of background which can be tolerated depends on the particular autoradiographic experiment which is being performed. As a rule of thumb, if the concentration of background silver grains exceeds 5 % of the concentration of real autoradiographic grains then some procedure must be developed to account for its effects.[37]

For background determination in this work, photomicrographs of the autoradiographs were prepared. Areas of blank formvar over the grids and areas of empty embedding resin adjacent to the tissue sections were photographed. It was found that the grain densities in these areas were essentially zero. Thus, the effects of background level on the distribution of real autoradiographic grains could safely be ignored.

Preparation of Photomicrographs for Image Analysis

Photomicrographs of the EM autoradiographs were prepared for image analysis. The photomicrographs were taken at a magnification of 4,800X. The electron microscope was operated at an accelerating voltage of 60 KV. Objective aperture No.2 was used. Prints were made on 11 X 14 inch paper at 20,690X. The magnification was calibrated using a lined grating replica with 2,160 lines/mm (Ernest Fullam Inc. Latham, NY.).

The photographic fields were selected to include only mature tracheids which had developed entirely during the precursor feeding period. These tracheids were

located in a swath which ran in the tangential direction, parallel to the cambium. The swath had a radial dimension of 2 to 3 tracheids. On the cambial side of the swath existed immature tracheids which had not yet deposited their S3 layers. On the pith side of the swath existed mature tracheids which had been developing prior to the beginning of the precursor administration period. These tracheids were identified by the very low (or zero) grain densities in their ML and P layers.

IMAGE ANALYSIS

IMAGE SPREAD

The basic autoradiographic process was described on p. 23. Excluded from this description was the concept that two types of error can occur during the production of an autoradiographic image. The first type stems from the fact that a radioactive decay particle may travel in any direction from the original isotope. As a result, a decay particle may strike a silver halide crystal some distance away causing a grain to form adjacent to the original isotope rather than immediately above it. This lateral displacement from the original isotope to the silver halide crystal is termed the geometric error. A second type of error may occur during development. As the silver grain grows from the point of the latent image it can actually grow to occupy an area outside the original silver halide crystal. Thus the center of the grain does not necessarily coincide with the center of the original silver halide crystal. The distance between these two centers is termed the photographic error. Figure 7 illustrates these two types of error.

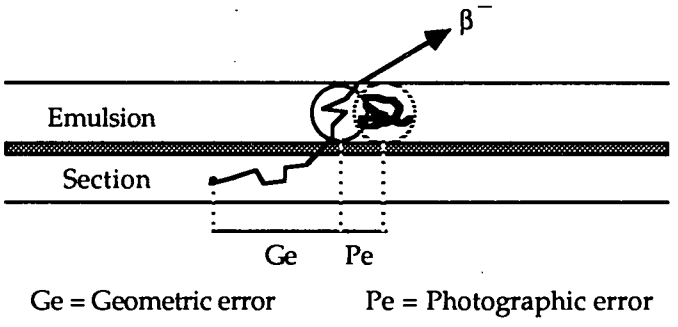

Figure 7. Two sources of error in autoradiography.

The geometric and photographic errors combined create the phenomenon of "image spread". The extent to which image spread occurs in an autoradiographic system is a function of five variables. These are: the autoradiographic emulsion type, the developer type, the type of radioisotope serving as the decay particle source, the thickness of the tissue section, and the thickness of the emulsion layer.

An emulsion with large silver halide crystals will have greater image spread than an emulsion with small silver halide crystals. The larger the crystal size the greater the contribution of the the photographic error. Developer type affects image spread in the same way. Developers which produce large silver grains have greater photographic error than those which produce small grains.

The effect of radioisotope on image spread is related directly to the average energy of their decay particles. Lower energy decay particles have shorter path lengths and consequently contribute less to geometric error. β^- particles emitted from tritium have approximately one tenth the average energy of those emitted from carbon 14. As a result autoradiographs made using tritium have less image spread than those using carbon 14.

Section thickness and emulsion layer thickness affect image spread in the same manner. Increasing the the thickness of either of these layers increases the maximum distance that can exist between an isotope and the silver halide crystals in the emulsion layer. This causes a corresponding increase in the potential geometric error.

MEASUREMENT OF IMAGE SPREAD

The degree of image spread for a given autoradiographic system is often expressed as half radius or HR. HR is defined as the distance from a point source of radiation within which half of the resulting silver grains fall. Figure 8a shows what an autoradiograph of a point source of radiation would look like. The silver grains are densely packed directly over the point source and become more dispersed farther away from the point source. The HR is the radius of a circle centered around the point source which encompasses half of the total number of grains. Also shown in Figure 8b is the point source density function or PSDF, which is a plot of grain density versus distance for an autoradiograph of a point source.

The HR and PSDF for several different autoradiographic systems have been determined experimentally and are reported in the literature. The EM autoradiographic system used in this investigation (summarized in Table 10) has a HR of 246.5 nm[38,39].

Table 10. Electron microscope autoradiographic system.

Variable	This system
radioisotope	tritium
emulsion	Ilford L4
developer	Kodak D19
section thickness	100 nm
emulsion layer thickness	170 nm

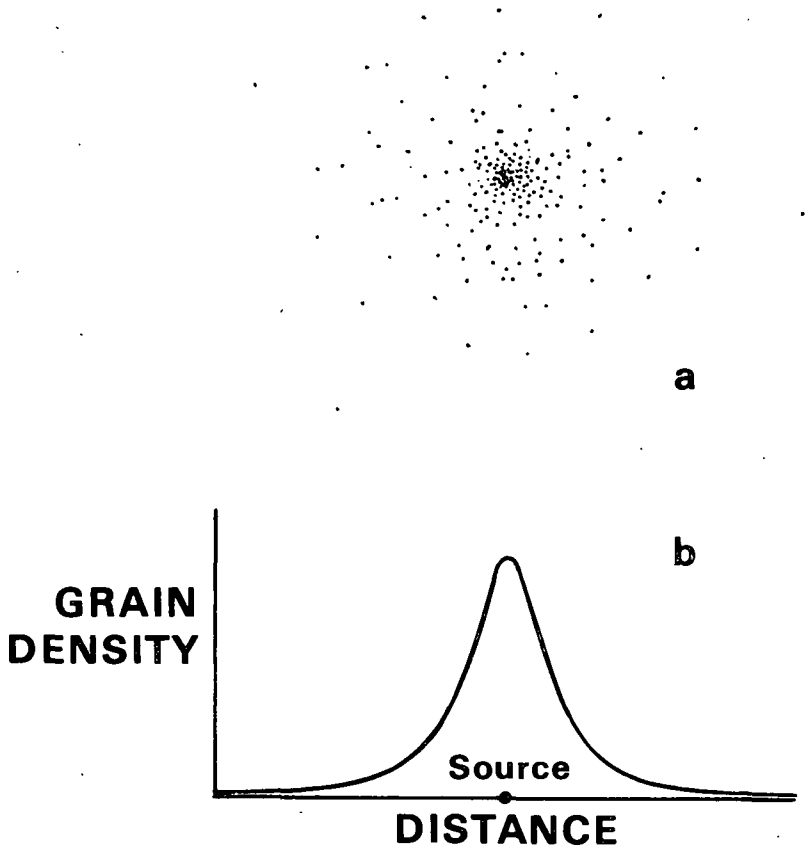

Figure 8. Distribution of autoradiographic grains around a point source.

THE NEED FOR IMAGE ANALYSIS

The effect of image spread on the analysis of autoradiographs is quite serious. As a result of image spread, radioactive isotopes in one area of an autoradiograph may cause grains to form over the top of another area. For example, a tritium atom in the S1 layer could decay and its resulting β^- particle could strike a silver halide crystal overlaying the S2 layer. When developed and viewed, this autoradiograph would contain one silver grain overlaying the S2 layer and no silver grains over

the S1.

The correct interpretation of this autoradiograph is not a straight forward task. One can not simply count the total number of silver grains overlaying each cell wall layer and use this as a measure of the radioactivity in that layer. This would lead to the erroneous assessment that the S2 was radiolabeled and the S1 was not. The effects of image spread must be taken into account when converting the distribution of silver grains over the cell wall into the distribution of radioactivity which exists in the cell wall layers.

There are several different image analysis techniques in the literature which attempt to account for the image spread inherent in the system. Most of these techniques are based on the same principles. The technique which was used in this investigation was developed by Blackett and Parry[40]. It, like the others, first obtains estimates for the probabilities that radiation in any tissue component causes the formation of silver grains overlaying any other component. It then uses these probabilities to work backward from the observed silver grain distribution to the real radioactivity distribution.

In the example above, the Blackett and Parry image analysis technique would first determine the probability that tritium atoms in the S1 would cause grains to form over the S2 and the probability that tritium atoms in the S2 would cause grains to form over the S1. Knowing this, the concentrations of radioactivity in the S1 and the S2 which would produce a distribution of silver grains like the one observed could be determined.

THE BLACKETT AND PARRY ANALYSIS TECHNIQUE

The EM photomicrographs were analyzed using the hypothetical grain method of Blackett and Parry [40]. The method consists of constructing a model of the EM autoradiographs. The model is used to test a series of scenarios concerning possible radioactivity distributions within the tissue section. The experimenter uses the model to determine the distribution of autoradiographic grains which would be formed over the surface of the tissue section from a proposed distribution of radioactivity within the section. The autoradiographic grain distribution predicted by the model is then compared to the real autoradiographic grain distribution which was observed in the experiment. The Chi squared goodness of fit between the model predicted autoradiographic distribution and the real grain distribution is then calculated. If an acceptable goodness of fit is obtained, the distribution of radioactivity within the tissue section determined by the model is accepted as a measure of the real radioactivity distribution within the sections.

If an acceptable goodness of fit is not obtained, a new model is defined by the experimenter and a new model predicted autoradiographic grain distribution is generated from it. This new grain distribution is then compared compared to the real autoradiographic grain distribution which was observed in the experiment and the Chi squared goodness of fit is calculated. The process of model refinement and testing is repeated until an acceptable goodness of fit is obtained. The distribution of radioactivity within the tissue section determined by the best model is then accepted as a measure of the real radioactivity distribution within the sections.

The first step in the Blackett and Parry analysis is the construction of the

model. The model describes the physical layout of the autoradiographs and the image spread that occurs within them. The model is constructed by the experimenter with reference to the actual photomicrographs. The model provides a way for the experimenter to identify and categorize every type of tissue component within the sections which could possibly contain radioactivity. It also provides a way to identify and categorize every location on the surface of the tissue section where autoradiographic grains could form.

This is accomplished by dividing all the components of the autoradiographs into two overlapping subsets. The first set is termed the set of sources. Each source is made up of a distinct cell wall layer or group of layers which could possibly contain radioactivity. The radioactivity within any one source is considered to be uniformly distributed. The entire set of sources must be selected such that any point in a photomicrograph could be assigned to one and only one source.

The second subset is termed the set of sites. The sites are discrete locations on top of the tissue section where autoradiographic grains could be located. Autoradiographic grains, unlike tritium atoms, occupy finite areas and could therefore overlay the border of two or more sources at one time. The sites however, must be defined in such a manner that any autoradiographic grain in the photomicrograph can be contained in one and only one site. Therefore, there are necessarily more components in the set of sites than in the set of sources. In addition to each source component serving as a site, the junction regions of two or more source components must be classified as individual sites. For the purpose of the model, the area occupied by a silver grain was defined as a circle with a radius equal to 246.5 nm. This corresponds to a radius of 5 mm at the 20,690 X

magnification of the photomicrograph prints.

Having defined the model, that is the components in the set of sources and the components in the set of sites, the next step in the analysis is to determine the probability that a radioactive decay event in any source component would produce an autoradiographic grain in any site component. This is accomplished by referring to the known distribution of autoradiographic grains which would occur around a point source of radioactivity for the specific autoradiographic system that was used. By making the initial assumption that each source component contains the same number of radioactive point sources on a per unit area basis and that these point sources are evenly distributed within each source, the number of autoradiographic grains which would be produced in each of the site components can be determined.

The number of hypothetical grains which occur in each site component can than be manipulated by changing the concentration of point sources which are assumed to reside within any given source. The concentration of point sources within each source of the model are manipulated so that the number of hypothetical grains which would reside in each site matches, as closely as possible the number of real grains which were observed in each site in the actual autoradiographs. The goodness of fit between the two grain distributions, hypothetical and real are measured by the Chi squared test.

If an acceptable fit is not obtained than the model is refined and the process is repeated. A model can be refined by redefining the components in the set of sources and in the set of sites. An acceptable model will be one which can accurately describe the image spread that is occurring between the sources and the sites. The concentration of radioactivity, or hypothetical point sources, proposed in each

source in the best fitting model are accepted as a measure of the concentration of radioactivity in the corresponding components in the actual autoradiographs.

In the next section the Blackett and Parry image analysis method is illustrated. The data used in this example is from the first model proposed for the L-(1-^{3}H)-arabinose fed trees.

AN ILLUSTRATION OF THE BLACKETT AND PARRY TECHNIQUE

The first model proposed in the analysis of the L-(1-^{3}H)-arabinose fed trees consisted of six sources and fourteen sites. The sources included the middle lamella (ML), the primary wall and the S1 layer combined (1), the outer half of the S2 layer (2o), the inner half of the S2 layer (2i), the S3 layer (3), and the lumen (L). Note that the S2 layer was divided geometrically into two parts with the division being a line located midway between the S1S2 interface and the S2S3 interface.

The sites consisted of the one component items: L, 2i, 2o, 1, and ML, the two component items: L/3, 3/2i, 2i/2o, 2o/1, and 1/ML, and the three component items: L/3/2i, 3/2i/2o, 2i/2o/1, and 2o/1/ML. The possible sites were identified by placing a 5 mm radius circle on top of the prints. The cell wall components which existed in this circle defined the site which the circle overlaid. If the circle contained only S1 layer material then the circle was overlaying the site 1. If the circle contained S1 and S2o layer material then the circle was overlaying the site 2o/1. If the circle contained ML, S1, and S2o layer material then the circle was overlaying the site 2o/1/ML. In this way all fourteen possible sites were identified. Note that the S3 is not listed as a one component site because it was not large enough to fill the entire

5 mm radius circle.

Having defined the model i.e. the set of 6 sources and the set of 14 sites, a hypothetical grain analysis matrix was generated to define the probability that a radioactive decay in any source would produce a grain overlaying any site. This was accomplished through the use of a Blackett and Parry type overlay. The overlay (obtained from Dr. John Baker[41]) consists of a regular array of identical 5 mm radius circles. Each circle has ten points located in and around it. The points represent hypothetical radioactive decay events and the circles represent the sites of the resulting hypothetical silver grains. The overlay corresponds to the specific EM autoradiographic system used in this investigation and to the 20,690 X magnification at which the prints were made. A photograph of the overlay is shown in Figure 9.

The construction of an overlay is described in detail in the literature.[39,40,42] The distance from a decay point to the center of its corresponding circle on the overlay was determined mathematically by randomly sampling the integral curve for the distribution of grains around a point source of tritium. The frequency with which any point to circle distance occurs on the overlay is therefore equal to the probability of a disintegration from a point source producing a grain at this distance away. The direction from the point to the center of the circle was determined by randomly sampling 16 different possible directions.

The overlay was used to generate the hypothetical grain matrix as follows. The overlay was placed directly on the surface of the photomicrographs and a series of hypothetical isotope decays and their corresponding hypothetical grain sites were recorded in matrix form. The resulting hypothetical grain matrix for all of the

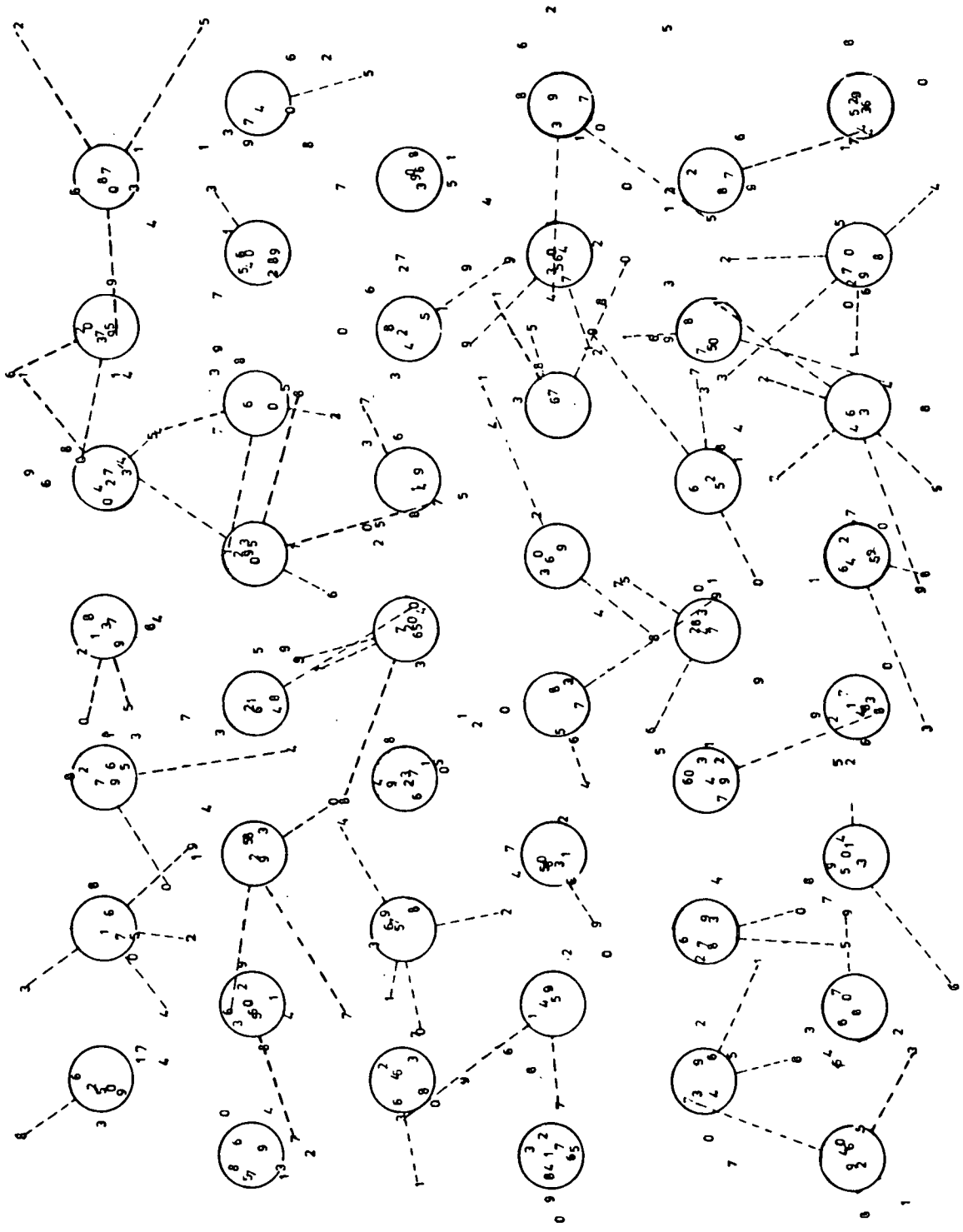

Figure 9. Blackett and Parry type overlay.

photomicrographs analyzed from the L-(1-^{3}H)-arabinose fed trees is shown in Table 11.

Table 11. Hypothetical grain analysis matrix for the first model of the L-(1-^{3}H)-arabinose fed trees.

	L	2i	2o	1	ML	L3	32i	2i2o	2o1	1ML	L32i	32i2o	2i2o1	2o1ML	Total
L	7170	13	2	0	0	438	64	10	9	1	228	8	5	0	7947
3	74	25	4	1	0	118	113	46	8	8	261	7	1	0	666
2i	56	343	42	3	1	59	315	596	57	28	213	40	9	2	1746
2o	14	50	469	26	5	11	43	589	689	115	32	19	31	21	2114
1	1	7	45	296	23	3	8	88	688	821	22	6	10	49	2067
ML	1	0	4	19	115	0	0	6	43	343	4	0	0	7	542

Sites are listed across the top. Sources are listed down the side.

The matrix is read in the following way. Referring to the upper left cell, 7170 hypothetical isotope decays occurred in the lumen (source L) which produced hypothetical silver grains overlaying the lumen (site L). Referring to the second cell in the top row, 13 hypothetical decays occurred in the lumen (source L) which produced hypothetical silver grains overlaying the inner half of the S2 (site 2i). Alternatively, the matrix can be read with reference to the total number of hypothetical decays which occurred in a given source. Referring to the first, second, and last cells in the top row, 7170 out of 7947 hypothetical decays which occurred in the lumen (source L) produced hypothetical grains which overlaid the lumen (site L). Thirteen out of 7947 decays which occurred in the lumen (source L) produced grains overlaying the inner half of the S2 (site 2i). The probability of a decay occurring in the lumen and producing a grain overlaying the lumen is therefore 7170/7947 or 0.902, while the probability of a decay occurring in the lumen and

producing a grain overlaying the inner half of the S2 is only 13/7947 or 0.00164.

The hypothetical grain matrix defines the probability that a decay occurring in any source will produce a grain overlaying any site. Note that the probability of a grain being produced in some sites is quite low for some sources and higher for others.

This matrix was generated by placing the overlay directly on top of each photomicrograph (Figure 10). The points associated with each circle identified the source of the hypothetical decay and the circle itself identified the site where the resulting hypothetical grain was formed. During each application of the overlay to a print only one point (or hypothetical source) was used for each circle. During the first application of the overlay only the point numbered 1 (associated with each circle in Figures 9 and 10) was used to identify the source. After all of the data for the circle - point number 1 pairs was recorded the overlay was moved to a new location on the photomicrograph and the data was collected from the circle - point number 2 pairs. This process was repeated until enough hypothetical grain data had been collected to adequately describe the image spread in the system.

By moving the overlay to a different location on the print for each set of circle - point pairs, a large area of the photomicrograph was sampled. This process was repeated for each photomicrograph. Some additional details on the generation of the hypothetical grain matrix are given in Appendix III. Also, a detailed description of the proper use of the Blackett and Parry overlay is given in their article.[40]

After generating the hypothetical grain matrix, the next step in the analysis

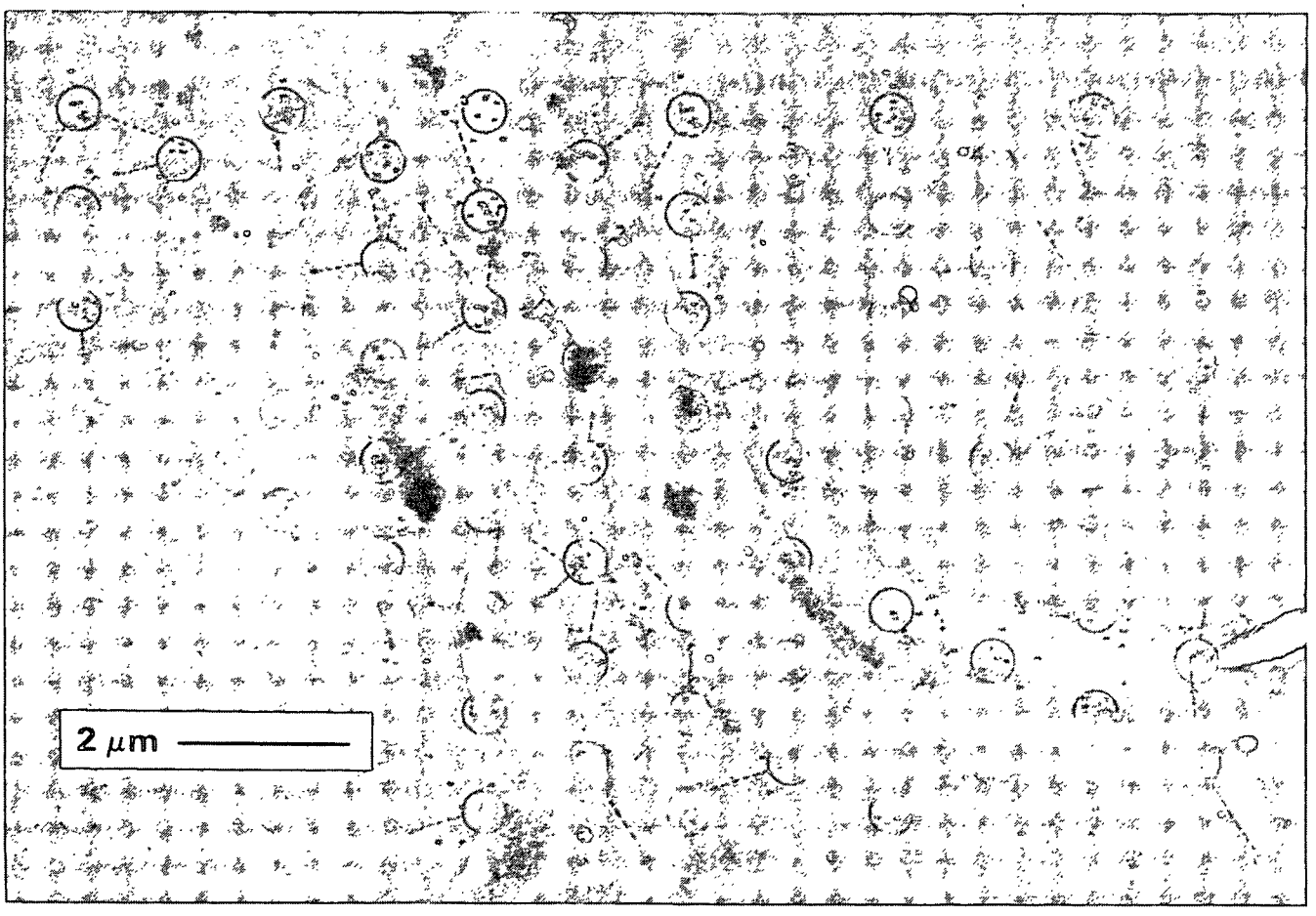

Figure 10. Overlay applied to a photomicrograph.

was to collect the real grain data. This was accomplished by centering a 5 mm radius circle, the same size as those on the overlay, around each real silver grain in the photomicrographs and recording the site contained in the circle. The process was performed on each photomicrograph. Unlike the collection of hypothetical data this procedure had to be performed only once. The real grain data for the L-(1-^{3}H)-arabinose fed trees is shown in Table 12.

Table 12. Hypothetical grain analysis matrix and real grain data for the first model of the L-(1-^{3}H)-arabinose fed trees.

	L	2i	2o	1	ML	L3	32i	2i2o	2o1	1ML	L32i	32i2o	2i2o1	2o1ML
L	7170	13	2	0	0	438	64	10	9	1	228	8	5	0
3	74	25	4	1	0	118	113	46	8	8	261	7	1	0
2i	56	343	42	3	1	59	315	596	57	28	213	40	9	2
2o	14	50	469	26	5	11	43	589	689	115	32	19	31	21
1	1	7	45	296	23	3	8	88	688	821	22	6	10	49
ML	1	0	4	19	115	0	0	6	43	343	4	0	0	7
HG	7316	438	566	345	144	629	543	1335	1494	1316	760	80	56	79
RG	83	107	94	144	47	66	127	378	452	523	160	20	9	33

Sites are listed across the top. Sources are listed down the side.
HG = the total number of hypothetical grains residing in each site as a result of all the hypothetical decays in all the sources.
RG = real grains overlaying each site (total for all photomicrographs).

Also included in Table 12 is the total hypothetical grain data (HG) for each site. This was obtained by summing each column in the original matrix. The HG data generated from the model could now be compared with the RG data by means of the Chi squared statistic (Equation 1) to determine if the model produced a distribution of hypothetical grains similar to the distribution of real grains.

$$\chi^2 = \sum_{i=1}^{k} \frac{(Oi - Ei)^2}{Ei} \qquad (1)$$

where Oi = observed frequency, Ei = expected frequency, and k = no. of classes

For this application the observed frequency is the real grain data and the expected frequency is the hypothetical grain data. A quick reference to the HG and

RG data in Table 12 reveals that a total Chi squared for these two data sets would be enormous. This is due to the fact that many more hypothetical grains were generated than the number of real grains which were collected. To make the Chi squared test fair the HG data should first be normalized to the total number of real grains collected.

The way in which the hypothetical data were normalized requires some explanation. It is first necessary to digress. Up to this point the analysis has included the inherent assumption that all of the sources contain the same concentration of radioactivity. This assumption was built into the generation of the hypothetical grain matrix.

Every time a point on the overlay fell on top of a source, a hypothetical isotope decay was said to occur in that source. The points were arranged in a regular array on the overlay and the overlay was placed on the photomicrographs in an unbiased fashion. Therefore, the larger the area a source occupied on the photomicrograph the greater the chance that a point on the overlay would fall on it. This is why there are so many more hypothetical grains originating in the lumen (source L) than in the middle lamella (source ML). From Table 11, 7947 hypothetical decays occurred in the lumen while only 542 occurred in the ML. The number of hypothetical decays occurring in a source is actually a measure of the size of the source relative to the other sources.

When the total number of hypothetical grains occurring in each site was determined (by summing each column) the assumption was made that each source contained the same radioactivity per unit area. Each source contained the same

number of hypothetical decays (or overlay points) on a per unit area basis.

The assumption that each source contains the same radioactivity per unit area is not necessarily true. In fact, this is the very question the autoradiography study was designed to answer. If the true radioactivity concentration of a source was known, from some outside information, then the number of hypothetical decays occurring in that source could be adjusted accordingly.

For example, if it was somehow known that the lumen contained only half the radioactivity on a per unit area basis as the other components then the total number of hypothetical decays occurring in the lumen could be multiplied by a factor of 0.5 to bring the model closer to reality. This would mean multiplying the hypothetical grains in each site in the top row of the matrix by 0.5.

Returning to the Chi squared test, it can now be seen that each row in the hypothetical grain matrix should be normalized independent of the others. For the matrix in Table 12, each row should be multiplied by some factor such that when the columns are summed and the total Chi squared is determined for the HG and RG data the total Chi squared value is minimized. The correct multiplying factor for each row (or source) which produces this minimum total Chi squared is thus a measure of the radioactivity per unit area of that source.

The correct multiplying factor for each row is determined by solving 14 simultaneous equations (14 = number of columns) for 6 unknowns (6 = number of rows, each row has one multiplying factor). This formidable task was performed by a computer program (obtained from Dr. Morton Maser[43]) using an iterative minimizing subroutine. The result of this process for Table 12 is shown in Table 13.

Table 13. Normalized hypothetical grain analysis matrix and Chi squared data for the first model of the L-(1-^{3}H)-arabinose fed trees.

	L	2i	2o	1	ML	L3	32i	2i2o	2o1	1ML	L32i	32i2o	2i2o1	2o1ML
L	40	0	0	0	0	2	0	0	0	0	1	0	0	0
3	22	7	1	0	0	35	33	13	2	2	77	2	0	0
2i	17	106	13	0	0	18	98	185	17	8	66	12	2	0
2o	2	7	71	3	0	1	6	90	105	17	4	2	4	3
1	0	3	20	136	10	1	3	40	318	379	10	2	4	22
ML	0	0	1	5	36	0	0	1	13	107	1	0	0	2
HG	83	125	108	148	47	59	142	332	457	516	161	20	12	28
RG	83	107	94	144	47	66	127	378	452	523	160	20	9	33
$\chi 2$	0	2	1	0	0	0	1	6	0	0	0	0	0	0

Total $\chi 2$ = 15.2 with 8 degrees of freedom.

Sites are listed across the top. Sources are listed down the side.
HG = the total number of hypothetical grains residing in each site as a result of all the hypothetical decays in all the sources.
RG = real grains overlaying each site (total for all photomicrographs).

Note that no values to the right of the decimal place are shown in the matrix, in the HG data, or in the individual χ^2 data. The values to the right of the decimal place were used by the computer program in the calculations but were not included in the computer printout. The values printed out by the program were not rounded off to the ones column. Instead, everything to the right of the decimal point was dropped off in the printout. This is a minor flaw of the computer program.

The multiplying factors for each row are shown in Table 14. Each row in Table 12 was multiplied by its corresponding factor in Table 14 to yield the adjusted HG data in Table 13. These factors are a measure of the radioactivity per unit area of

each source. The units of each factor are real grains per hypothetical grain (RG/HG).

Table 14. Source multiplying factors for the first model of the L-(1-^{3}H)-arabinose fed trees.

Source	Description	Factor
L	lumen	0.006
3	S3 layer	0.298
2i	inner half of the S2 layer	0.311
2o	outer half of the S2 layer	0.153
1	S1 + primary layer combined	0.462
ML	middle lamella	0.314

As shown in Table 14 the model predicted a different radioactivity concentration for each source. The S1 + primary layers were found to have the highest concentration of radioactivity while the lumen was found to have the lowest concentration. This marked the end of step 3 in the Blackett and Parry analysis of the first model of the L-(1-^{3}H)-arabinose fed trees.

MODEL ASSESSMENT AND REFINEMENT

The first model (or set of sources and sites) proposed in the Blackett and Parry analysis method may not necessarily produce a good fit with the real grain data. After the first solution is found it may be necessary to redefine the model to achieve an acceptable fit. The method provides a basis for model refinements via the Chi squared test. An examination of the sites which contribute the greatest amounts to the total chi squared will reveal where the model fails and will suggest how it should be changed.

The first model produced a total Chi squared of 15.2 with 8 degrees of freedom corresponding to a probability of $0.05 < P < 0.06$. Stated another way, the probability of a real grain distribution arising by chance from the radioactivity distribution described in Table 14 producing a χ^2 this large is between 5 and 6 in 100. Note that the degrees of freedom was defined as the number of sites minus the number of sources. In their article Blackett and Parry[40] incorrectly defined the degrees of freedom as the number of sites minus 1. This mistake was pointed out in the literature by Salpeter *et al.*.[44]

The Chi squared test as used in this analysis determined the confidence level at which the model could be rejected. The confidence level is defined as $100(1-\alpha)\%$ where α = the probability (P) determined from the Chi squared function. A probability of $P = 0.06$ corresponds to a confidence level of 94%. At this confidence level the decision to reject the model carries with it only a 6 in 100 chance of being wrong. This is termed the probability of committing a Type I error.

The probability of committing a Type 2 error can not be determined by this analysis. A Type 2 error occurs when the decision is made to accept a model which is in reality false. In the above example if the decision to accept the model is made, the probability of this being an incorrect decision can not be determined. This probability is not the inverse of the Type 1 probability. There is not simply a 94% chance of committing a Type 2 error. This probability depends on the degree of falseness of the model and as such is entirely unknown.

The probability level for the first model was not very good. The model could be rejected with only a small risk of being wrong. For this type of analysis a

probability level of approximately 50% is considered good.[40] At this level, the probability of a real grain distribution arising by chance from the model radioactivity distribution and producing a χ^2 this large is 1 in 2. Therefore, if the radioactivity distribution determined by the model was actually correct and the entire autoradiographic experiment was repeated several times the resulting χ^2 values would be larger than the 50% probability value in half of the replicates.

Based on the result of the Chi squared test, the decision was made to refine the first model and repeat the Blackett and Parry analysis. A model can be refined in several ways. Sources can be added to or deleted from a model. Two or more sources can be combined into one larger item, or one large source can be broken down into smaller items. These same changes can also be made to sites categories. An examination of the individual Chi squared values suggested where the present model failed most. In Table 13, the largest individual Chi squared value is in the site 2i2o. The model predicted significantly fewer grains in this category then were actually observed. In the next model this could perhaps be corrected by creating a new source category, the central part of the S2 layer or by recombining the sources 2i and 2o into one category consisting of the entire S2 layer. Many other model refinements were also possible.

The process of refining the model and repeating the Blackett and Parry analysis was carried out several times until a model which produced an acceptable fit with the real grain data was obtained. The source multiplying factors for this best fitting model were then accepted as a measure of the radioactivity concentrations of the individual sources. The results of the Blackett and Parry analysis of the best model for each set of trees, the L-(1-^{3}H)-arabinose trees and the D-(2-^{3}H)-mannose

trees, are described in the Results and Discussion section.

ESTIMATION OF ERROR VALUES

The computer program which determined the multiplying factors for each source also employed Monte Carlo techniques to determine pseudo error values for these factors. True error values can not be obtained without repeating the experiment on several sets of trees. It is possible however to obtain estimates for the errors that would be expected if the statistical variation in the counting procedure of real and hypothetical grains were the only source of error.

This was accomplished by the computer program in the following way. Poisson distributions with means equal to each value in the original matrix and each RG value for the sites were generated. An entirely new matrix of hypothetical grains and a new set of real grains was then obtained by randomly sampling these Poisson distributions. The iterative minimizing routine was then performed on this new set of data to obtain the values for its source multiplying factors. This process was repeated 100 times. The standard deviation was then determined for the values of the source factors.

RESULTS AND DISCUSSION

IDENTIFICATION OF LABELED CELL WALL COMPONENTS

Radioactivity in Klason Lignin

Samples of Klason lignin prepared from labeled wood were subjected to liquid scintillation counting. The percent of the total radioactivity in the xylem attributable to the lignin was determined (Table 15). The total activity for each sample was based on the combined activities of its hydrolyzate and Klason lignin. The two values for tree 2 originated from separate wood samples taken from different stem locations. In the L-(1-^{3}H)-arabinose fed trees less than 1% of the total activity was present in the lignin. In the D-(2-^{3}H)-mannose fed trees less than 2% of the total activity was present in the lignin.

Table 15. Radioactivity in Klason lignin.

Tree	Tritiated Precursor	DPM/mg	% Activity In Lignin
2	ARA	37	0.23
2	ARA	72	0.30
8	ARA	152	0.43
7	MAN	79	1.80
4'	MAN	30	1.40

DPM/mg = disintegrations per minute per mg of lignin.

Radioactivity in the Monosaccharides

The hydrolyzates were separated into individual monosaccharides by preparative layer chromatography. The following monosaccharides were identified

and isolated: galactose, glucose, mannose, arabinose, and xylose. Each of these monosaccharides was subjected to liquid scintillation counting. Any material which remained at the origin of the PLC plates was also isolated and counted. Material which is not mobile in this chromatographic system consists of galacturonic acid, glucuronic acid, aldobiuronic acid, and aldotriuronic acid. Also, any dimers or trimers resulting from the incomplete hydrolysis of the polysaccharides would remain near the origin.

L-(1-^{3}H)-Arabinose Fed Trees

4.5% (average of 3 samples) of the radioactivity in the hydrolyzate of this wood remained at the origin. Each of the five monosaccharides from the hydrolyzate of L-(1-^{3}H)-arabinose fed wood contained measurable radioactivity. Over 50 % of the label contained in the monosaccharides was present in arabinose (Figure 11). The remaining activity was spread rather evenly amongst the four other monosaccharides.

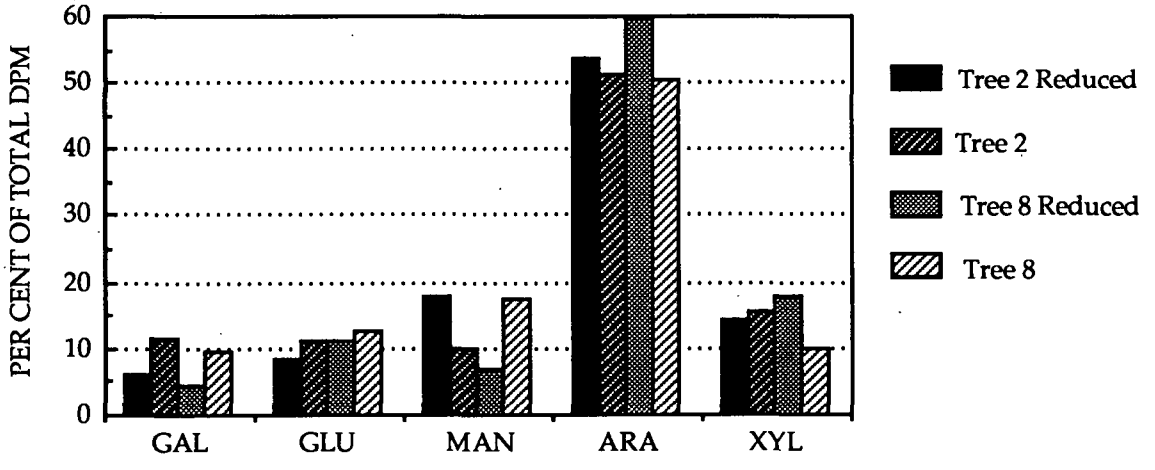

Figure 11. Distribution of activity in the monosaccharides of L-(1-^{3}H)-arabinose fed wood.

The effect of reducing the wood prior to hydrolysis can be seen by comparing the percentage of the total activity present in the arabinose with and without reduction. The borohydride reduction would have converted any free unmetabolized L-(1-^{3}H)-arabinose into arabitol which would then have been separated from the arabinose during chromatography. A large decrease in the arabinose activity of the reduced wood could then be interpreted as evidence for the presence of a significant amount of umetabolized precursor. As illustrated in Figure 11, no decrease occurred in the relative activity of the arabinose as a result of the borohydride reduction.

D-(2-^{3}H)-Mannose Fed Trees

12.4% (average of 2 samples) of the radioactivity in the hydrolyzate of this wood remained at the origin of the PLC plates. Each of the five monosaccharides contained measurable radioactivity. Approximately 50% of the label contained in the monosaccharides was present in the mannose (Figure 12). The next largest fraction was in glucose followed by galactose. Lesser activities were found in the pentoses.

The results of the sodium borohydride reduction test showed that a significant amount of unmetabolized D-(2-^{3}H)-mannose was not present in this wood. This reduction would have caused any free unmetabolized D-(2-^{3}H)-mannose to be converted to its mannitol form. The mannitol would then have been separated from the mannose during chromatography. As illustrated in Figure 12 a significant decrease did not occur in the relative activity of the mannose as a result of this reduction step.

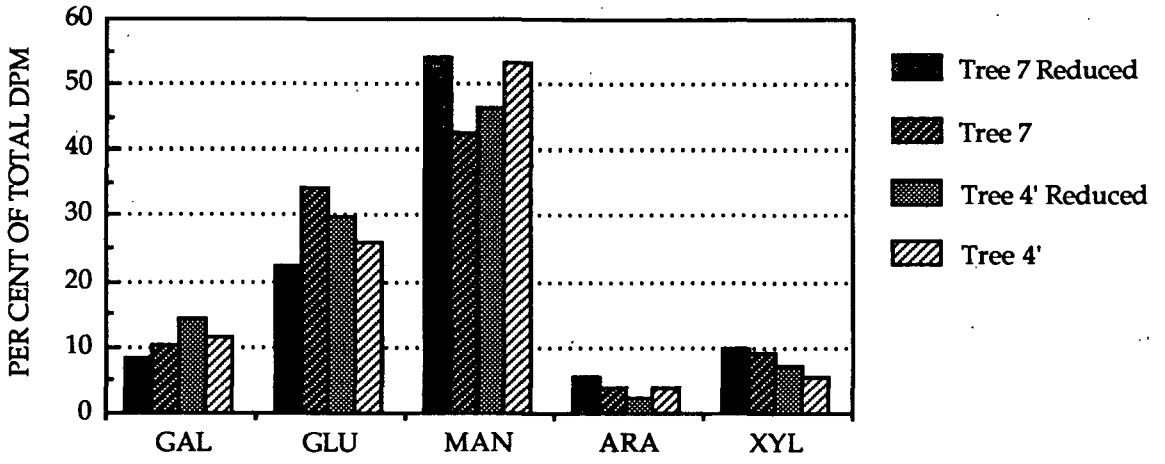

Figure 12. Distribution of activity in the monosaccharides of D-(2-^{3}H)-mannose fed wood.

Discussion of the Liquid Scintillation Work

The results of the liquid scintillation work show that the two precursors have preferentially labeled the hemicelluloses in the xylem. Neither precursor proved to be quite as specific in this system as previous shorter-term studies had shown them to be in other systems.[22, 23, 24, 25, 26] The tritium label was incorporated to some extent into each of the five monosaccharides. A very small amount of label was also incorporated into the Klason lignin. The exact reason for this lower specificity is not known. However, the precursors were administered to the trees for a much longer period of time in this study than in the previous studies. This extended period may have enabled the precursors to enter several different pathways which were not encountered in the shorter pulse feeding studies.

Each precursor labeled a different fraction of hemicelluloses. The L-(1-^{3}H)-arabinose precursor labeled a large fraction of pentoses; arabinose and xylose account for an average of 68% of the total label present in the monosaccharides. The

D-(2-^{3}H)-mannose precursor labeled a large fraction of hexoses; galactose, glucose, and mannose account for an average of 88% of the total label present in the monosaccharides of these trees.

It is not surprising that each of the monosaccharides contain at least a small amount of radiolabel. The actions of specific epimerases can cause conversions between the hexose sugars and between the pentoses sugars. In addition to this, hexoses can be converted to pentoses by the action of a dehydrogenase to form the corresponding hexuronic acid. This can then be followed by the action of a decarboxylase to form a pentose sugar. Conversions from a pentose sugar to a hexose sugar could occur via photosynthesis. Photosynthesis would be necessary to supply the additional carbon atom to the pentose sugar forming the hexose sugar.[45]

Each precursor produced some labeled glucose : 11% in the L-(1-^{3}H)-arabinose trees, 28% in the D-(2-^{3}H)-mannose trees. It is not certain if this represents labeled cellulose or labeled glucose-containing hemicelluloses such as galactoglucomannan, xyloglucan, and others. If a small amount of labeled cellulose is present, the distribution of radioactivity across the cell wall would still reflect, to a greater extent, the distribution of labeled hemicelluloses.

The exact source of the radioactivity in the Klason lignin was not determined. The results in Table 15 indicate however that the activity is probably due to labeled lignin and not labeled carbohydrate bound to the lignin in a lignin-carbohydrate complex. The support for this theory is based on the different lignin activity levels for the two treatments. The D-(2-^{3}H)-mannose fed wood has a 4 to 5 times greater relative activity in its Klason lignin than the L-(1-^{3}H)-arabinose fed wood. If this

activity were due to labeled carbohydrate one would expect the Klason lignin of the L-(1-^{3}H)-arabinose fed wood to have the higher activity. The L-(1-^{3}H)-arabinose labeled a large fraction of arabinosyl units. Arabinosyl units are common in pectin and it is the pectin which is generally thought to bind with the lignin in the lignin-carbohydrate complex.

Since however, the higher activity was found in the Klason lignin of the D-(2-^{3}H)-mannose fed wood, the most likely explanation is that this activity represents actual labeled lignin. The difference between the two treatments could reflect the more direct biosynthetic route from a hexose sugar to lignin than from a pentose sugar to lignin. A pentose sugar must go through the pentose phosphate pathway to form D-erythrose 4-phosphate, a lignin precursor. A hexose sugar on the other hand can be converted directly to D-erythrose 4-phosphate by glycolysis.[46]

The results of the sodium borohydride reduction test were encouraging. This experiment showed that the tritium had actually been incorporated into the cell wall polysaccharides. A significant quantity of labeled free monosaccharide was not present in the xylem. Thus, the distribution of radioactivity revealed by the autoradiography work was truly a distribution of radioactive polymers and not simply a distribution of unmetabolized precursors.

ANALYSIS OF AUTORADIOGRAPHS

L-(1-^{3}H)-Arabinose Fed Trees

The first model proposed in the analysis of the of the L-(1-^{3}H)-arabinose fed trees was described in the Image Analysis section. This model consisted of 6 sources

and 14 sites. It produced a fit with the real grain data that could be rejected at the 94% confidence level. Several different model refinements were then tested before an acceptable model was found. The final model consisted of 5 sources and 10 sites.

Two of the sources present in the original model were combined into one large source in the final model. The inner half of the S2 layer (source 2i) and the outer half of the S2 layer (source 2o), were combined into one source consisting of the entire S2 layer (source 2). The related site categories were also combined. The one component sites 2i and 2o and the junctional region two component site 2i/2o were combined into one site made up of the entire S2 layer (2). The two component site 3/2i and the three component site 3/2i/2o were combined into the site 3/2. Sites 2o/1 and 2i/2o/1 were combined into site 2/1.

The five sources present in the final model therefore included the lumen (L), the S3 (3), the S2 (2), the S1 plus the primary layer combined (1), and the middle lamella (ML). The ten sites present in the final model consisted of the one component items: L, 2, 1, and ML, the two component items: L/3, 3/2, 2/1, and 1/ML, and the three component items: L/3/2 and 2/1/ML. The hypothetical grain analysis matrix for this model is shown in Table 16. This matrix was obtained by combining the corresponding rows and columns in Table 12.

Table 16. Hypothetical grain analysis matrix and real grain data for the best model of the L-(1-^{3}H)-arabinose fed trees.

	L	2	1	ML	L3	32	21	1ML	L32	21ML
L	7170	24	0	0	438	72	14	1	228	0
3	74	75	1	0	118	120	9	8	261	0
2	70	2089	29	6	70	417	786	143	245	23
1	1	140	296	23	3	14	698	821	22	49
ML	1	10	19	115	0	0	43	343	4	7
HG	7316	2338	345	144	629	623	1550	1316	760	79
RG	83	579	144	47	66	147	461	523	160	33

Sites are listed across the top. Sources are listed down the side.
HG = the total number of hypothetical grains residing in each site as a result of all the hypothetical decays in all the sources.
RG = real grains overlaying each site (total for all photomicrographs).

The correct multiplying factor for each source which produces the best match of the hypothetical grain data to the real grain data was determined by the computer program. These source factors are a measure of the radioactivity per unit area of each source. The source factors along with their respective error values are listed in Table 17. As shown, the model predicts the S1 + primary layer to have the highest concentration of radioactivity followed by the S3, the ML, the S2, and lastly, the lumen. Also included in this table are the relative areas and relative activities of each source. These values were calculated by the program according to the formulas shown in Table 17.

Table 17. Source multiplying factors for the best model of the L-(1-^{3}H)-arabinose fed trees.

Source	Description	Source Factors	Relative Activity	Relative Area
L	lumen	0.005 ±0.001	1.9 ±0.1	52.6 ±1.0
3	S3 layer	0.371 ±0.010	11.0 ±0.8	4.4 ±0.4
2	S2 layer	0.228 ±0.005	39.4 ±0.7	25.7 ±0.2
1	S1 + primary layer	0.426 ±0.022	39.3 ±1.5	13.7 ±0.3
ML	middle lamella	0.349 ±0.069	8.4 ±1.6	3.6 ±0.2

$$\text{Relative Area} = \frac{\text{no. of hypothetical disintegrations in a source}}{\text{no. of hypothetical disintegrations in all sources}} \times 100$$

$$\text{Relative Activity} = \frac{\text{(Relative Area x Source Factor) for a source}}{\text{the sum of the (Relative Area x Source Factor) for all sources}} \times 100$$

The normalized matrix for this model is shown in Table 18. Each row in Table 16 was multiplied by its corresponding source factor in Table 17 to yield the normalized matrix in Table 18. As discussed before (p. 59) values to the right of the decimal point were not included in this matrix. They were, however, used in the calculations.

The best model for the L-(1-^{3}H)-arabinose fed trees produced a total Chi squared of 4.6 with 5 degrees of freedom. This corresponds to a probability of P = 0.46. The decision to reject this model therefore carries with it a 46 in 100 chance of being wrong. This is a more than satisfactory level at which to accept the model.

Table 18. Normalized hypothetical grain analysis matrix and Chi squared data for the best model of the L-(1-^{3}H)-arabinose fed trees.

	L	2	1	ML	L3	32	21	1ML	L32	21ML
L	38	0	0	0	2	0	0	0	1	0
3	27	27	0	0	43	44	3	2	96	0
2	15	475	6	1	15	94	178	32	55	5
1	0	59	126	9	1	5	297	349	9	20
ML	0	3	6	40	0	0	14	119	1	2
HG	83	566	139	51	63	145	494	504	164	28
RG	83	579	144	47	66	147	461	523	160	33
χ^2	0	0	0	0	0	0	2	0	0	0

Total $\chi 2$ = 4.6 with 5 degrees of freedom.

Sites are listed across the top. Sources are listed down the side.
HG = the total number of hypothetical grains residing in each site as a result of all the hypothetical decays in all the sources.
RG = real grains overlaying each site (total for all photomicrographs).

D-(2-^{3}H)-Mannose Fed Trees

The first model proposed in the analysis of the D-(2-^{3}H)-mannose fed trees was identical to the first model proposed for the L-(1-^{3}H)-arabinose fed trees. The hypothetical grain analysis matrix consisted of the same 6 sources and 14 sites and is shown in Appendix IV. The hypothetical and real grain data in this matrix were of course collected from the photomicrographs of the D-(2-^{3}H)-mannose fed trees and as such are different from the data in the first matrix of the L-(1-^{3}H)-arabinose fed trees.

The first model for the D-(2-^{3}H)-mannose fed trees produced a fit with the real grain data that could be rejected at the 99.9% confidence level. Several different

model refinements were then tested before an acceptable model was found. The final model consisted of 5 sources and 11 sites.

One source present in the original model, the middle lamella (source ML) was completely removed from the final model. When the ML was included as a source in the model its activity was determined to be essentially zero (within experimental error). Removing the ML from the list of potential sources, i.e. considering it to be completely unlabeled, resulted in a better fitting model.

Alterations were also made to the sites of the original model. Some smaller three component sites were combined into related one component sites to reduce the scatter and improve the fit. The site 3/2i/2o was combined into the site 2i. Site 2i/2o/1 was combined into the site 2o. Site 2o/1/ML was combined into the site 1. These combinations were made on the morphological basis that each of the three component sites consisted almost entirely of the middle component (located in the central part of an overlay circle) with a much smaller amount of the other two components (located in the circle periphery). Combining the three component sites into their associated one component sites reduced the matrix from 14 to 11 columns. The reduced Chi squared gained by simplifying the model in this way outweighed the penalty associated with loosing three degrees of freedom.

The 11 sites present in the final model therefore consisted of the one component items: L, 2i, 2o, 1, and ML, the two component items: L/3, 3/2i, 2i/2o, 2o/1, and 1/ML, and the three component item L/3/2i. The 5 sources present in the final model included the lumen (L), the S3 (3), the inner half of the S2 (2i), the outer half of the S2 (2o), and the S1 plus the primary layer combined (1). The hypothetical

grain analysis matrix for this model is shown in Table 19. This matrix was obtained by completely removing the row ML and by combining the appropriate columns in the matrix of the first model for the D-(2-^{3}H)-mannose fed trees shown in Appendix IV.

Table 19. Hypothetical grain analysis matrix and real grain data for the best model of the D-(2-^{3}H)-mannose fed trees.

	L	2i	2o	1	ML	L3	32i	2i2o	2o1	1ML	L32i
L	4295	15	0	0	0	320	25	18	2	3	154
3	36	17	4	2	0	72	65	24	14	6	159
2i	26	268	49	4	0	43	206	403	48	19	138
2o	9	51	309	32	2	7	26	363	425	69	18
1	3	4	47	240	14	6	4	50	476	534	16
HG	4369	355	409	278	16	448	326	858	965	631	485
RG	28	93	132	72	6	17	68	282	312	180	68

Sites are listed across the top. Sources are listed down the side.
HG = the total number of hypothetical grains residing in each site as a result of all the hypothetical decays in all the sources.
RG = real grains overlaying each site (total for all photomicrographs).

The correct multiplying factor for each source which produces the best match of the hypothetical grain data to the real grain data was determined by the computer program. These source factors along with their respective error values are listed in Table 20. As shown, the model predicts the outer half of the S2 to have the highest concentration of activity and the inner half of the S2 to have the second highest. These are followed in descending order by the S1, the S3, and the lumen. Also included in this table are the relative areas and relative activities of each source. Table 21 shows the normalized matrix and Chi squared data for this model.

Table 20. Source multiplying factors for the best model of the D-(2-^{3}H)-mannose fed trees.

Source	Description	Source Factors	Relative Activity	Relative Area
L	lumen	0.003 ±0.001	1.2 ±0.6	52.9 ±1.4
3	S3 layer	0.065 ±0.033	2.0 ±1.0	4.4 ±0.3
2i	inner half of the S2 layer	0.283 ±0.025	27.1 ±1.9	13.2 ±0.4
2o	outer half of the S2 layer	0.378 ±0.005	39.4 ±1.6	14.3 ±0.4
1	S1 + primary layer	0.273 ±0.014	30.2 ±0.8	15.3 ±0.3

$$\text{Relative Area} = \frac{\text{no. of hypothetical disintegrations in a source}}{\text{no. of hypothetical disintegrations in all sources}} \times 100$$

$$\text{Relative Activity} = \frac{\text{(Relative Area x Source Factor) for a source}}{\text{the sum of the (Relative Area x Source Factor) for all sources}} \times 100$$

Table 21. Normalized hypothetical grain analysis matrix and Chi squared data for the best model of the D-(2-^{3}H)-mannose fed trees.

	L	2i	2o	1	ML	L3	32i	2i2o	2o1	1ML	L32i
L	13	0	0	0	0	1	0	0	0	0	0
3	2	1	0	0	0	4	4	1	0	0	10
2i	7	75	13	1	0	12	58	114	13	5	39
2o	3	19	116	12	0	2	9	137	160	26	6
1	0	1	12	65	3	1	1	13	129	145	4
HG	27	97	143	78	4	22	73	266	304	177	61
RG	28	93	132	72	6	17	68	282	312	180	68
χ^2	0	0	0	0	0	1	0	0	0	0	0

Total χ^2 = 5.7 with 6 degrees of freedom.

Sites are listed across the top. Sources are listed down the side.
HG = the total number of hypothetical grains residing in each site as a result of all the hypothetical decays in all the sources.
RG = real grains overlaying each site (total for all photomicrographs).

Each row in Table 19 was multiplied by its corresponding source factor in Table 20 to yield the normalized matrix in Table 21. Recall that values to the right of the decimal point were used in the calculations but do not appear in the matrix. The best model for the D-(2-^{3}H)-mannose fed trees produced a total Chi squared of 5.7 with 6 degrees of freedom. This corresponds to a probability of P = 0.45. The decision to reject this model therefore carries with it a 45 in 100 chance of being wrong. The model was accepted at this level.

Discussion of the Blackett and Parry Analysis Models

The Lumen as a Source

What was and was not considered to be a "source" in the models requires some explanation. The lumen was considered to be a source by each model. For each set of trees the lumen was predicted to contain a very low level of radioactivity.

When the lumen (source L) was removed from each model, the fit obtained with the real grain data was far worse. The models predicted far fewer hypothetical grains in the lumen (site L) then the numbers of real grains which were observed there. This contributed significantly to the total Chi squared and resulted in a higher confidence level at which the model could be rejected.

Including the lumen as a potential source made it much easier for the model to account for the real grains observed in the lumen. The concentration of radioactivity predicted in the lumen for each set of trees was extremely low compared to the concentrations predicted in the other cell wall layers. In the L-(1-^{3}H)-arabinose trees the concentration of radioactivity in the lumen was

between 1.2 - 2.2 percent of the concentration present in any of the cell wall layers. In the D-(2-^{3}H)-mannose trees the concentration of radioactivity in the lumen was between 0.8 to 4.6 percent of the concentration found in the cell wall layers.

Two possible explanations for the radioactivity predicted in the lumens were immediately ruled out. The first was the possibility that the lumens could actually be radioactive. Some radioactive compounds present in the cell wall could have leached out of the cell wall and into the embedding resin causing the resin in the lumens to be radioactive. This is very unlikely considering the extensive washing procedure each wood block under went prior to embedding. Also, the inspection of areas of blank resin adjacent to the wood sections in the autoradiographs revealed no measurable concentration of silver grains.

The second possibility was that the predicted radioactivity concentration in the lumen was due to background exposures from outside sources. This possibility however was ruled out by a determination of the background level in the autoradiographs. The background level was so low as to be unmeasurable.

The most likely explanation for the predicted radioactivity in the lumen stems from the nature of the analysis technique which was employed. The Blackett and Parry overlay which was used to describe the image spread in this system was based on the image spread around a point source of radioactivity. The overlay however, contained only a finite number of hypothetical source - grain pairs.

The image spread around a point source contains a wide spectrum of distances. The curve contains a long right hand tail which results from the small

percentage of grains that can form at extremely long distances away from the point source. While the major portion of the curve is easy to define and can be accurately described by the Blackett and Parry overlay, the long tail region is not. An accurate description of the tail region in the overlay would require an unmanageable amount of data.

When this limitation is considered together with the very large size of the lumen (over 50 % of the total area in each set of trees) one can see that if the analysis method were to fail it would likely first fail in describing this situation. Image spread from anywhere within the cell wall to the lumen is a relatively long distance. This type of long distance spread was probably slightly underestimated by the Blackett and Parry analysis method. As a result, fewer hypothetical grains were recorded over the lumen then the number of real grains which were observed. The models interpreted this as meaning that the lumen was slightly radioactive.

The Middle Lamella as a Source

The middle lamella was not listed as a source in the best model of the D-(2-^{3}H)-mannose fed trees. When it was included as a source in the model the concentration of radioactivity in the middle lamella was determined to be zero (within experimental error). By removing the middle lamella as a potential source an additional degree of freedom was added in the model. Recall that the degrees of freedom were defined as the number of sites minus the number of sources. Adding a degree of freedom to the model decreased the confidence level at which the model could be rejected.

The S2 as a Source

In the first models for each set of trees the S2 layer was divided into two separate sources representing the inner and outer halves of the S2 layer. This division was made based on evidence in prior cell wall studies that the hemicellulose content may vary within this layer.[10] The S2 was also the only cell wall layer large enough to make this division practical from a data collection standpoint.

The division of the S2 layer produced a better fitting model for the D-(2-^{3}H)-mannose trees. In the L-(1-^{3}H)-arabinose trees the opposite proved true. With these trees, dividing the S2 into separate sources resulted in a poorer fitting model.

INTERPRETATION OF THE AUTORADIOGRAPHY RESULTS

The analysis of the EM autoradiographs determined the relative concentration of radioactivity in each cell wall layer. The distributions of activity for each treatment were significantly different. Neither precursor produced an even distribution of radioactivity across the cell wall. In the L-(1-^{3}H)-arabinose fed trees (Figure 13) the concentration of radioactivity increased from the middle lamella to the combined primary + S1 layers. It decreased significantly in the S2 layer and then increased to its previous level in the S3 layer. The D-(2-^{3}H)-mannose fed trees, on the other hand, showed a peak of radioactivity in the middle of the cell wall (the S2o) which decreased sharply at the inner and outer layers of the cell wall (Figure 14).

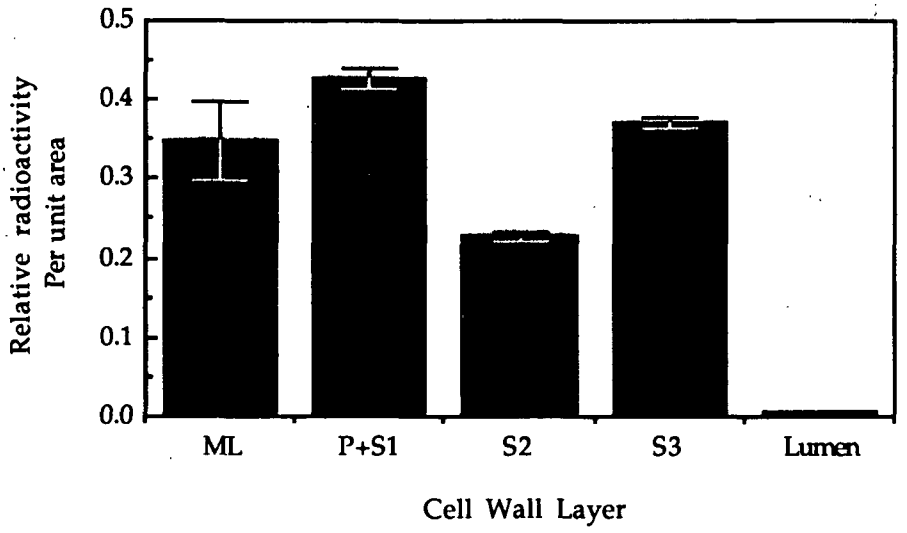

Figure 13. Distribution of activity in the cell walls of the L-(1-^{3}H)-arabinose fed trees

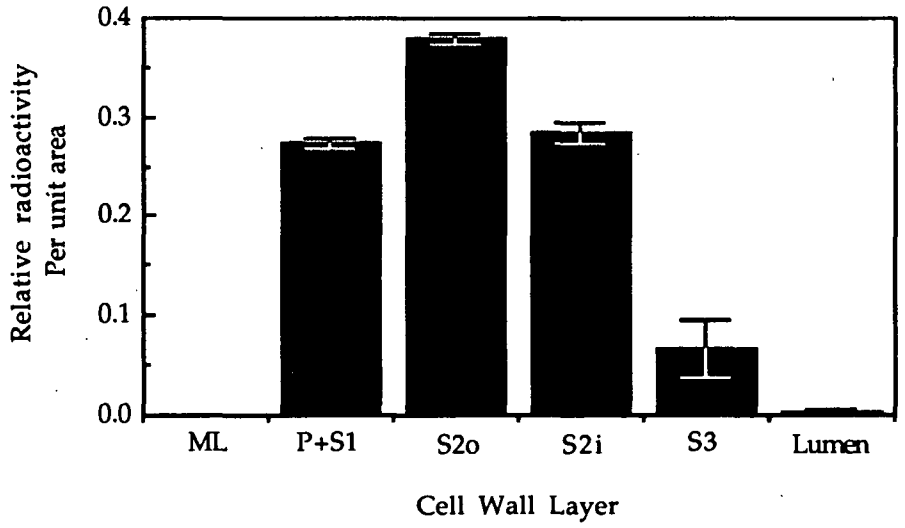

Figure 14. Distribution of activity in the cell walls of the D-(2-^{3}H)-mannose fed trees

The values plotted in Figures 13 and 14 are the source factors which were obtained from the best fitting model for each set of trees. The units for these values are real grains per hypothetical grain (RG/HG). The values in Figure 13 were taken from Table 17 and the values in Figure 14 were taken from Table 20. Note that it is

not possible to compare the absolute values of the source factors between the two sets of trees. Comparisons of these values can only be made within a set of trees.

The interpretation of the radioactivity distribution across the wall is complicated by the fact that the activity in any one cell wall layer could be caused by several different radiolabeled polysaccharides. The liquid scintillation counting analysis showed that each of the five major monosaccharides contained at least some radiolabel. Together these monosaccharides could be present in several different types of hemicellulose. We therefore can not say with certainty that the radioactivity in a given cell wall layer is due to one specific radiolabeled hemicellulose.

However, it is reasonable to assume that the distribution of activity in the L-(1-^{3}H)-arabinose fed trees reflects mainly the distribution of radiolabeled arabinose. We therefore would expect, from the previous studies, to find the highest concentration of activity in the ML and P layers.[9, 10, 16, 18] Note that in this study the P layer was grouped with the S1 into one category whereas, in the previous studies, the P layer was grouped with the ML. Based on the distribution of arabinose from the previous studies, this classification difference would cause the P + S1 layer in this study to have a higher concentration of activity than the S1 layer would normally have on its own.

The concentrations of radioactivity in the S2 and S3 layers were much higher than would be expected based on their previously reported arabinose contents alone. The elevated activity in these layers may reflect the presence of the other monosaccharides which were labeled by this precursor. According to the results of

Meier[9] and Côté *et al.*[10], labeled mannose and labeled xylose would be expected to contribute more to the activity level of the secondary wall than to the middle lamella or primary wall. Alternatively, the observed level of radioactivity in the S2 and S3 layers may be an indication that the arabinose content of the secondary cell wall was underestimated by the previous studies.

The distribution of activity in D-(2-^{3}H)-mannose fed trees corresponds well to the mannose distribution determined by Meier[9] and Côté *et al.*[10] for each cell wall layer excluding the S3. In those studies the mannose concentration was found to increase sharply from the compound middle lamella to the S1 and to increase at a lower rate from the S1 to the S2. While in this study no radioactivity was detected in the middle lamella, it again differs from the previous studies in that the primary layer was grouped with the S1 and not with the middle lamella. The mannose content in the compound middle lamella of the previous studies may have been due to its presence in the primary layer alone. If this were the case, grouping the primary layer with the S1 in this study would have reduced the concentration of radioactivity observed in the middle lamella to zero.

There is a large discrepancy over the mannose concentration of the S3 layer between this study and the others. The previous studies[9, 10] predict a much higher mannose concentration in the S3 than this study found. One possible explanation for this is that some of the mannose attributed to the S3 layer in the previous studies was actually being intussusceptively deposited into the S1 or S2 while the S3 layer was forming. The allocation of this material to the S3 layer in their analysis would have overestimated the mannose content of that layer.

There is additional evidence that the mannose content is lower in the S3

layer than in the S2. In a study of the glucomannan-synthase activity in the differentiating cells of pine (*Pinus sylvestris* L.) Dalessandro *et al.*[47] isolated glucomannan-synthase containing particulate membrane preparations from xylem cells at three different stages of development. The first fraction of cells consisted of cambial cells with thin primary walls. Fraction 2 consisted of cells at different stages of secondary thickening. Fraction 3 consisted of cells which were completing secondary thickening or which had just completed it.

The specific activity of the enzyme prepared from each of these fractions was measured by monitoring the rate at which it polymerized ^{14}C-mannose into ^{14}C-mannan. It was found that the activity on a per cell basis was 2 to 4 times higher in fraction 2 cells than in fraction 1 cells. Also, the specific activity was slightly lower in the fraction 3 cells than in the fraction 2 cells in three of the four cell fraction sets which were tested. This variation in the glucomannan synthase activity with the maturity of the cells provides a basis for understanding how the D-(2-^{3}H)-mannose administered in this study could have been incorporated into the cell wall with the observed activity distribution.

The EM autoradiographic analysis performed in this investigation has contributed significantly to the understanding of the hemicellulose distribution across the cell wall. The results presented here depict a cell wall which is far from uniform in its hemicellulose content. Each cell wall layer contains a different proportion of hexose and pentose containing hemicelluloses. This investigation has confirmed the results of previous studies which have suggested that the pectins are the predominant hemicelluloses in the middle lamella. It has also presented new evidence that the middle lamella is entirely devoid of mannan and that the

mannan content of the S3 is greatly diminished relative to that of the S2.

CONCLUSIONS

A new method for visualizing the distribution of hemicelluloses within the tracheid cell wall was developed. A split stem feeding technique was successfully used to supply solutions of tritium labeled hemicellulose precursors to the cambial region of 3 and 4 year old red pine for an extended period of time. This feeding technique allowed some tracheids to develop entirely in the presence of the precursor.

Two different radiolabeled hemicellulose precursors, L-(1-^{3}H)-arabinose and D-(2-^{3}H)-mannose, were used. Analysis of the resulting labeled wood determined that a different fraction of polysaccharides had been labeled by each precursor. The L-(1-^{3}H)-arabinose labeled a fraction rich in pentoses with L-arabinose accounting for over 50% of the total activity present in the monosaccharides of the hydrolyzate. D-(2-^{3}H)-mannose labeled a fraction rich in hexoses. Approximately 49% of the activity in the monosaccharides in this wood hydrolyzate was present in D-mannose units.

The production and analysis of EM autoradiographs revealed that the cell wall distributions of radioactivity produced by each precursor were significantly different. The L-(1-^{3}H)-arabinose fed tracheids contained higher concentrations of radioactivity at the inner and outer layers of the cell wall than in the S2 layer. Conversely, the D-(2-^{3}H)-mannose fed tracheids contained their highest concentration of radioactivity in the S2 layer and much lower concentrations in the inner and outer cell wall layers. No radioactivity was detected in the middle lamella of the tracheids which received this precursor. These results indicate that the

hemicelluloses are not evenly distributed across the cell wall. The hexose and pentose containing hemicelluloses are present in different proportions in each cell wall layer.

RECOMMENDATIONS

The results of this work have demonstrated the value of long term radiotracer studies. It is possible to produce wood cells that have fully developed in the presence of radiolabeled chemicals. The split stem feeding technique coupled with electron microscope autoradiography provides a method for studying the chemical composition of the cell wall in a relatively unaltered state. Greater knowledge of the chemical composition of the cell wall could lead to a better understanding of the cell wall deposition process, the physical and chemical properties of the cell wall, and the function of the cell wall within the tree.

A recommended avenue for future work is to use these techniques in studies with other labeled precursors. In the area of hemicelluloses, a specific xylan precursor could provide valuable information on the distribution of xylan in the cell wall of both softwoods and hardwoods. In the area of lignin chemistry, specific lignin precursors could provide a more detailed understanding of the distributions of guaiacyl and syringyl lignin. Because of the very long incubation periods required in this type of study, it would be necessary to determine the specificity of any precursor used.

ACKNOWLEDGEMENTS

The author wishes to express his gratitude to Dr. R.A. Atalla, Dr. M.A. Johnson and Dr. N.S. Thompson, the members of the thesis advisory committee, for their interest and contributions. The collective wealth of their knowledge was indispensable. The author is especially grateful to Dr. Thompson for remaining an active member of this committee even through his retirement.

The advice, encouragement, and contributions of Dr. J.R. Baker of Ciba-Giegy Pharmaceuticals concerning the delicate science of autoradiography is greatly appreciated. Additionally, the author wishes to thank Dr. M.D. Maser of Woods Hole Educational Associates for his contribution of the HGP analysis program.

Financial support from the member companies of the Institute of Paper Chemistry is gratefully acknowledged.

Finally, I would like to thank my wife Deirdre for her support and encouragement. Her diligent proof reading and editing enhanced the quality of this manuscript.

LITERATURE CITED

1. Panshin, A.J.; de Zeeuw, C. Textbook of Wood Technology. 4th. ed. McGraw-Hill, New York, NY 1980: 74-78.

2. Goodwin, T.W.; Mercer, E.I. Introduction to Plant Biochemistry. 2nd ed. Pergamon Press, Oxford, England 1983: 58-76.

3. Lange, P.W., Svensk Papperstidn. 57,525(1954).

4. Browning, B.L. The Chemistry of Wood. Interscience Publishers, New York, NY, 1963: 68-69.

5. Luce, J.A., Pulp and Paper Magazine of Canada. October:T419-T423(1964).

6. Bailey, A. J., Industrial and Engineering Chemistry. 8(5):389-391(1936).

7. Sultze, R. F., Tappi. 40(12):985-994(1957).

8. Meier, H.; Wilkie, K.C.B., Holzforschung 13(6):177-182(1959).

9. Meier, H., Journal of Polymer Science 51:11-18(1961).

10. Côté, W. A.; Kutscha, N. P.; Simson, B. W.; Timell, T. E., Tappi. 51(1): 33-39(1968).

11. Thompson, N. S.; Kremers, R. E.; Kaustinen, O. A., Tappi. 51(3):127-131(1968).

12. Ray, P. M., Journal of Cell Biology. 35:659-674(1967).

13. Mullis, R. H.; Thompson, N.S.; Parham, R. A., Planta. 132:241-248(1976).

14. Takabe, K.; Fujita, M.; Harada, H.; Saiki, H., Mokuzai Gakkaishi. 27(4): 249-255(1981).

15. Hardell, H.; Westermark, U., The Ekman-Days. Vol. 5. p.17-19. International Symposium on Wood and Pulping Chemistry, Stockholm, June 9-12, 1981.

16. Hardell, H.; Westermark, U., The Ekman-Days. Vol. 1. p. 32-34. International Symposium on Wood and Pulping Chemistry, Stockholm, June 9-12, 1981.

17. Whiting, P.; Favis, B. D.; St-Germain, F. G. T.; Goring, D. A. I., Journal of Wood Chemistry and Technology. 1(1):29-42(1981).

18. Whiting, P.; Goring, D. A. I., Can. J. Chem. 61:506-508(1983).

19. Johnson, D. B.; Moore, W. E.; Zank, L. C., Tappi. 44:793(1961).

20. Burke, D.; Kaufman, P.; McNeil, M.; Albersheim, P., Plant Physiol. 54:109(1974).

21. Whitmore, F. W.; Zahner, R., Forest Science. 12(2):198-210(1966).

22. Roberts, R. M., Arch. Biochem. 145:685-692(1971).

23. Mullis, R. H. An Autoradiographic Study of Pentosan Deposition in the Cell Walls of *Populus tremuloides* Michx. The Institute of Paper Chemistry, Appleton, WI 1975. pp. 27-29.

24. Roberts, R. M.; Butt, V. S., Planta. 94:175-183(1970).

25. Roberts, R. M.; Shah, R. H.; Loewus, F., Plant Physiology. 42:659-666(1967).

26. Loewus, F. A.; Jang, R., J. Biol. Chem. 232:521-532(1958).

27. Gude, W. D. Autoradiographic Techniques. Prentice-Hall, Inc., Englewood Cliffs, NJ 1968:1-6.

28. Cohen, E.; Arad, S.M.; Heimer, Y.M.; Mizrahi, Y., Plant Physiol. 70:540-543(1982).

29. Feirer, R., The Institute of Paper Chemistry, Personal communication, 1985.

30. Saeman, J. F.; Moore, W. E.; Mitchel, R. L.; Millett, M. A., Tappi. 37(8): 336-343(1954).

31. Iwakawa, J.; Kobatake, H.; Suzuki, I.; Kushida, H., J. of Chromatography. 193: 333-337(1980).

32. Hough, L.; Jones, J. K. N.; Wadman, W. H., J. Chem. Soc. 1702(1950).

33. Gentile, V.M., Effects of Physical Structure on the Alkaline Degradation of Hydrocellulose. The Institute of Paper Chemistry, Appleton, WI 1986. p. 92.

34. Gould, R. M.; Holshek, J.; Silverman, W.; Spivack, W., J. of Neurochemistry. 48(4): 1121-1131(1987).

35. Salpeter, M. M.; Bachman, L. Autoradiography. In Principals and Techniques of Electron Microscopy Biological Applications Vol. 2. Ed. Hayat, M. N., Van Nostrand Reinhold Co., NewYork, NY 1972:262-264.

36. Caro, L.; Van Tubergen, R.P., J. of Cell Biology. 15:173(1962).

37. Williams, M.A. Autoradiography and Immunocytochemistry. Elsevier/North-Holland Biomedical Press, Amsterdam,The Netherlands, 1977:110-117.

38. Salpeter, M.M.; Szabo,M., J. of Histochemistry and Cytochemistry. 20(6): 425-434(1972).

39. Salpeter, M.M.; Bachmann, L.; Salpeter, E.E., J. of Cell Biology. 41:16-17(1969).

40. Blackett, N.M.; Parry, D.M., J. of Histochemistry and Cytochemistry. 25(3): 206-214(1977).

41. Baker, J.R., Research Centre Ciba-Geigy Pharmaceuticals. Horsham, West Sussex, England, Personal communication, 1987.

42. Blackett, N.M.; Parry, D.M., J. of Cell Biology. 57:9-15(1973).

43. Maser, M.D., Woods Hole Educational Associates. Woods Hole, Mass. Personal communication, 1988.

44. Salpeter, M.M.; McHenry, F.A.; Salpeter, E.E., J. of Cell Biology. 76:127-145(1978).

45. Goodwin, T.W.; Mercer, E.I. Introduction to Plant Biochemistry. 2nd ed. Pergamon Press, Oxford, England 1983: 267-268.

46. Goodwin, T.W.; Mercer, E.I. Introduction to Plant Biochemistry. 2nd ed. Pergamon Press, Oxford, England 1983:79-82, 224.

47. Dalessandro, G.; Piro, G.; Northcote, D.H., Planta. 169:564-574(1986).

48. Nemec, J.; Kefurt, K.; Jary, J., J. of Chromatography. 26:116-120(1967).

APPENDIX I

ESTABLISHMENT OF A DPM PROGRAM

A stock solution of tritiated water produced by New England Nuclear on 2/2/83 was used to prepare a 50 ml working solution of tritiated water containing 0.7988mCi of radioactivity. Ten µl of this solution which corresponds to 354,674 DPM were placed into each of 12 liquid scintillation vials. Ten ml of cocktail were added to each vial and they were mixed on a vortex mixer. A solution consisting of 1g of tartrazine in 250 ml of water was prepared. This solution was used as a source of quench in the vials. A different volume was added to each vial. The vials were then remixed.

The vials were counted in the Beckman LS3801 liquid scintillation counter to a 2 sigma tolerance of 1 %. The quench curve was established automatically by the instrument and stored within its operating system. The quench curve is a plot of percent efficiency (vertical axis) versus H factor (horizontal axis). Percent efficiency equals (CPM / DPM) X 100 for a sample. The H-factor is a measure of the internal quench occurring in a sample. It is determined automatically by reference to an internal instrument radioactivity source of ^{137}cesium.

The coefficients for the quench curve function (2) are shown below. These mathematically define the quench curve.

$$\text{natural log of efficiency} = A + B(H\#) + C(H\#)^2 + D(H\#)^3 \qquad (2)$$

$A = 6.142070 \quad B = -0.030154 \quad C = 0.00010404 \quad D = -0.0000001866$

The data from which the quench curve was established are shown in Table 22. For each vial this table lists the µl of tartrazine solution added, the H-factor, the measured efficiency (determined from the measured CPM and the known DPM = 354,674), the calculated efficiency (determined from the quench curve using the measured CPM and the H-factor), and the percent difference between the measured the calculated efficiencies.

Table 22. Quench curve preparation and correlation data.

Sample Number	µl of Quench Solution	H#	Measured Efficiency	Calculated Efficiency	Percent Difference
1	0	152.7	25.97	26.44	1.78
2	0.5	157.0	25.16	25.15	-0.03
3	1.0	162.3	23.55	23.67	0.53
4	2.0	170.7	21.98	21.56	-1.88
5	3.5	180.0	19.63	19.45	-0.91
6	5.0	190.3	17.49	17.36	-0.71
7	7.5	207.3	14.23	14.38	1.09
8	10.0	224.7	11.67	11.78	0.91
9	15.0	253.7	8.12	8.17	0.65
10	20.0	279.0	5.65	5.64	-0.18
11	30.0	311.0	3.24	3.20	-1.09
12	40.0	373.7	0.67	0.67	-0.10

In addition to the quench curve, the DPM program used to convert the CPM data to DPM data included a background subtract function. The background CPM were determined for unlabeled monosaccharides. These monosaccharides were isolated from unlabeled wood using the same hydrolysis and preparative layer chromatography procedures that were used for the labeled wood. Six samples, counted to a 2 sigma tolerance of 5 %, had an average CPM of 18.42 with a range of

17.43 to 18.97. Based on these figures an automatic background subtraction of 18 CPM was included in the DPM program.

APPENDIX II

THIN LAYER CHROMATOGRAPHY DATA

Solutions of aldoses and alditols were prepared for thin layer chromatography. Five standard solutions, each containing galactitol, glucitol, mannitol, arabitol, or xylitol at 5 μg/μl were prepared. A solution containing all five alditols at 1 μg/μl each was also prepared. In addition, a solution containing 1 μg/μl each of the corresponding aldoses (galactose, glucose, mannose, arabinose, and xylose) was prepared.

One μl spots of each solution were applied to a 20 X 20 cm thin layer chromatography plate. The spots were applied in a horizontal line 1.5 cm from the bottom edge of the plate. The plates consisted of plastic sheets coated with 0.2 mm of silica gel 60. They were produced by E. Merck, Darmstadt G.F.R. and purchased from Brinkman Instruments, Westbury, NY. These thin layer plates differ only in the thickness of the silica gel layer from the preparative layer plates which were used for the separation of the actual hydrolyzates .

After spotting the plate was allowed to dry. Development was carried out in the same manner as before (p. 33). The plate was developed three times in the same direction in the ethyl acetate - pyridine - water solvent system. After development the spot detection technique of Nemec *et al.*[48] was used. The plate was sprayed first with a 0.42 % solution of potassium metaperiodate in water. Five minutes later, the plate was sprayed with a second solution. This solution consisted of 1.28 g of benzidine hydrochloride in 10 ml acetone and 50 ml of 50% aqueous ethanol. The resolved aldoses and alditols appeared as white spots on a deep blue background.

Note that these two spray reagents are very hazardous. They were sprayed using an aerosol can in a well ventilated hood. Plastic gloves were worn during the spraying and handling of the wet plates.

The distance traveled from the origin by each aldose and alditol was measured. The results are shown in Table 23. The RG value for each species is shown. RG is a dimensionless number defined as the distance traveled by the species divided by the distance traveled by glucose.

Table 23. Separation of aldoses and alditols.

SPECIES	RG
galactitol	0.67
glucitol	0.69
mannitol	0.75
galactose	0.75
glucose	1.00
xylitol	1.09
arabitol	1.20
mannose	1.24
arabinose	1.63
xylose	2.21

APPENDIX III

GENERATION OF HYPOTHETICAL GRAIN MATRICES

During each application of an overlay to a print only one hypothetical source point was used for each circle. The overlay was then reapplied to the print in a different location and the data for a different set of source point - circle pairs was collected. The overlay was applied to the print in a regular manner each time. It was not applied randomly.

The first application of the overlay was made to the lower left hand corner of the print. The second application was made to the upper right hand corner. The third application was made horizontally across the center of the print. Ten different possible applications of the overlay to the print were defined in this manner. Each print was subjected to the defined applications in the same order. In this way a large area of the photomicrographs was sampled.

The orientation of the tissue section in the photomicrographs was dependent on the orientation of the tissue section in the electron microscope and as such was entirely random. Applying the overlay to the photomicrographs in a systematic way preserved this randomness.

The overlay was reapplied to a print until a sufficient number of hypothetical grains had been collected. The goal in collecting hypothetical grains is to collect a sufficient number such that the error associated with collecting them is significantly smaller than the error associated with the collection of real grains. Error is associated with the collection of both real and hypothetical grains due to the random

process of how they are generated. These errors can be reduced by collecting larger numbers of grains, both real and hypothetical. On a practical level however the collection of real grains is limited by the duration of the autoradiographic exposure period. Additional numbers of hypothetical grains can always be collected by reapplication of the overlay.

According to the Blackett and Parry[40] at least twice as many hypothetical grains as real grains should be collected to insure that the generation of hypothetical grains is not the major source of error in the analysis. Others have suggested that hypothetical grains should be collected until the error values determined by the Monte Carlo technique are sufficiently small and the values predicted for the source factors converge.[41] In this study approximately 5.5 times as many hypothetical grains as real grains were collected.

Since the autoradiographs produced from each tree contained different real grain densities, it was necessary to reapply the overlay more times to some photomicrographs than to others to assure that a sufficient number of hypothetical grains per real grains were collected. The number of overlay applications made to any one photomicrograph varied from 2 to 10.

APPENDIX IV

HYPOTHETICAL AND REAL GRAIN DATA FOR EACH TREE

This appendix lists the hypothetical grain analysis matrices for the first model of each tree. Each matrix is identified by the line immediately above it. Included in this line are the tree number, the tissue block number(s), and the number of photomicrographs which were analyzed. The matrix for the first model of all the D-(2-^{3}H)-mannose fed trees combined is also listed. The corresponding matrix for the L-(1-^{3}H)-arabinose fed trees was listed on p. 63.

The following abbreviations are used in the tables. HG = the total number of hypothetical grains residing in each site as a result of all the hypothetical decays in all the sources. RG = the total number of real grains overlaying each site (total for all photomicrographs).

Table 24. Hypothetical grain analysis matrix and real grain data for the first model of the D-(2-^{3}H)-mannose fed trees.

	L	2i	2o	1	ML	L3	32i	2i2o	2o1	1ML	L32i	32i2o	2i2o1	2o1ML
L	4295	9	0	0	0	320	25	18	2	3	154	6	0	0
3	36	9	2	1	0	72	65	24	14	6	159	8	2	1
2i	26	223	39	4	0	43	206	403	48	19	138	45	10	0
2o	9	29	282	24	2	7	26	363	425	69	18	22	27	8
1	3	1	34	203	14	6	6	4	50	476	534	16	3	13	37
ML	0	1	1	2	12	103	1	0	4	28	265	0	2	3	12
HG	4369	272	359	244	119	449	326	862	993	896	485	86	55	58
RG	28	68	103	47	6	17	68	282	312	180	68	25	29	25

Table 25. Hypothetical grain analysis matrix and real grain data for tree 2, block 2D, 10 photos.

	L	2i	2o	1	ML	L3	32i	2i2o	2o1	1ML	L32i	32i2o	2i2o1	2o1ML
L	1059	5	2	0	0	72	12	0	0	0	28	2	0	0
3	15	7	2	1	0	23	22	9	1	2	42	2	0	0
2i	9	76	7	1	0	13	51	100	12	5	45	9	1	0
2o	2	13	96	8	0	2	9	111	137	25	4	3	3	1
1	1	0	14	66	7	1	1	17	130	163	2	0	1	2
ML	1	0	2	3	21	0	0	1	4	57	0	0	0	0
HG	1087	101	123	79	28	111	95	238	284	252	121	16	5	3
RG	10	27	19	34	10	15	38	42	78	109	22	0	0	4

Table 26. Hypothetical grain analysis matrix and real grain data for tree 4, blocks 4A and 4C, 10 photos.

	L	2i	2o	1	ML	L3	32i	2i2o	2o1	1ML	L32i	32i2o	2i2o1	2o1ML
L	885	0	0	0	0	48	8	0	2	0	44	0	0	0
3	5	5	1	0	0	11	9	4	0	1	31	0	0	0
2i	6	41	0	1	0	7	36	79	8	2	25	0	2	1
2o	0	5	62	4	0	0	5	73	78	12	4	1	2	1
1	0	1	1	26	4	0	1	12	92	107	2	0	4	7
ML	0	0	0	2	13	0	0	1	3	40	0	0	0	1
HG	896	52	64	33	17	66	59	169	183	162	106	1	8	10
RG	12	12	14	19	1	4	14	40	63	72	16	2	0	4

Table 27. Hypothetical grain analysis matrix and real grain data for tree 5, block 5B, 15 photos.

	L	2i	2o	1	ML	L3	32i	2i2o	2o1	1ML	L32i	32i2o	2i2o1	2o1ML
L	1158	6	0	0	0	79	12	2	0	0	20	0	0	0
3	8	5	1	0	0	33	31	7	1	0	45	0	0	0
2i	10	116	14	0	0	12	74	121	6	3	27	1	1	0
2o	0	17	145	0	1	1	6	119	112	19	1	0	3	4
1	0	2	13	43	2	0	0	8	107	130	0	0	0	10
ML	0	0	1	1	15	0	0	0	5	66	0	0	0	0
HG	1176	146	174	44	18	125	123	257	231	218	93	1	4	14
RG	7	37	27	10	9	13	15	59	62	100	25	0	0	9

Table 28. Hypothetical grain analysis matrix and real grain data for tree 8, block 8C, 13 photos.

	L	2i	2o	1	ML	L3	32i	2i2o	2o1	1ML	L32i	32i2o	2i2o1	2o1ML
L	2050	0	0	0	0	130	14	5	1	0	60	4	0	0
3	23	7	0	0	0	28	35	9	4	4	72	2	0	0
2i	11	58	14	0	1	12	98	162	15	11	51	17	2	0
2o	4	11	93	9	3	3	14	153	183	32	9	6	8	5
1	0	3	13	84	3	1	2	21	184	225	5	1	2	13
ML	0	0	1	6	31	0	0	1	17	106	2	0	0	2
HG	2088	79	121	99	38	174	163	351	404	378	199	30	12	20
RG	28	19	16	40	16	13	35	132	125	147	30	7	6	7

Table 29. Hypothetical grain analysis matrix and real grain data for tree 1', block 1'D, 5 photos.

	L	2i	2o	1	ML	L3	32i	2i2o	2o1	1ML	L32i	32i2o	2i2o1	2o1ML
L	2019	2	0	0	0	109	17	2	6	1	76	2	5	0
3	23	1	0	0	0	23	16	17	2	1	71	3	1	0
2i	20	52	7	1	0	15	56	134	16	7	65	13	3	1
2o	8	4	73	5	1	5	9	133	179	27	14	9	15	10
1	0	1	4	77	7	1	4	30	175	196	13	5	3	17
ML	0	0	0	7	35	0	0	3	14	74	2	0	0	4
HG	2070	60	84	90	43	153	102	319	392	306	241	32	27	32
RG	26	12	18	41	11	21	25	105	124	95	67	11	3	9

Table 30. Hypothetical grain analysis matrix and real grain data for tree 6, block 6C, 11 photos.

	L	2i	2o	1	ML	L3	32i	2i2o	2o1	1ML	L32i	32i2o	2i2o1	2o1ML
L	933	0	0	0	0	74	8	8	0	0	32	4	0	0
3	10	2	0	0	0	17	13	4	1	1	21	1	0	0
2i	9	49	5	2	0	7	38	76	8	2	21	10	3	0
2o	0	2	72	6	0	0	1	68	91	13	2	3	5	0
1	0	0	7	48	4	1	0	9	87	100	6	0	2	4
ML	0	0	0	3	18	0	0	1	5	55	0	0	0	0
HG	952	53	84	59	22	99	60	166	192	171	82	18	10	4
RG	2	19	18	10	0	3	10	44	54	24	10	2	3	1

Table 31. Hypothetical grain analysis matrix and real grain data for tree 7, blocks 7B and 7D, 11 photos.

	L	2i	2o	1	ML	L3	32i	2i2o	2o1	1ML	L32i	32i2o	2i2o1	2o1ML
L	850	6	0	0	0	45	2	4	0	0	37	0	0	0
3	5	2	0	0	0	8	10	1	1	0	33	0	0	0
2i	3	56	11	1	0	4	46	96	7	2	29	1	0	0
2o	2	9	73	6	0	2	8	65	99	6	4	2	0	1
1	0	0	6	58	1	1	2	5	104	112	1	0	0	2
ML	0	0	0	3	9	0	0	1	4	55	0	0	0	1
HG	860	73	90	68	10	60	68	172	215	175	104	3	0	4
RG	1	17	23	17	2	2	9	55	50	40	12	0	0	0

Table 32. Hypothetical grain analysis matrix and real grain data for tree 4', block 4'D, 17 photos.

	L	2i	2o	1	ML	L3	32i	2i2o	2o1	1ML	L32i	32i2o	2i2o1	2o1ML
L	1546	0	0	0	0	85	2	6	2	0	46	2	0	0
3	12	2	0	0	0	16	12	9	4	3	47	5	1	0
2i	8	20	4	1	0	15	49	91	17	8	52	29	2	0
2o	5	5	28	4	2	1	10	90	115	19	6	11	18	4
1	2	0	3	45	3	4	0	19	135	156	4	2	7	18
ML	0	0	1	1	26	0	0	1	9	61	0	2	2	5
HG	1573	27	36	51	31	121	73	216	282	247	155	51	30	27
RG	13	6	20	8	2	8	18	90	84	60	30	15	19	20

Table 33. Hypothetical grain analysis matrix and real grain data for tree 5', block 5B, 12 photos.

	L	2i	2o	1	ML	L3	32i	2i2o	2o1	1ML	L32i	32i2o	2i2o1	2o1ML
L	966	3	0	0	0	115	13	0	0	3	39	0	0	0
3	9	3	2	1	0	31	30	10	8	2	58	2	1	1
2i	6	98	19	0	0	17	73	140	16	7	36	5	5	0
2o	2	13	109	8	0	4	7	140	120	31	6	6	4	3
1	1	1	18	52	6	0	2	17	150	166	5	1	4	13
ML	0	1	1	5	50	1	0	1	10	94	0	0	1	6
HG	984	119	149	66	56	168	125	308	304	303	144	14	15	23
RG	12	26	42	12	2	4	31	93	124	56	16	8	7	4